



# Role of PBL and Microphysical Parameterizations During WRF Simulated Monsoonal Heavy Rainfall Episodes Over Mumbai

SAURABH VERMA,<sup>1</sup> JAGABANDHU PANDA,<sup>1</sup>  and SUDHANSU S. RATH<sup>1</sup>

**Abstract**—Monsoon circulation and associated rainfall add complexities in the boundary layer features over the Indian subcontinents. Besides relevant microphysical variables, the characteristics of various boundary layer parameters and their variations at differing spatial and temporal scales are investigated over Mumbai during monsoonal heavy rainfall scenarios. During the summer monsoon months (June to September) of 2014–2018, 16 heavy rainfall cases are chosen for this study. High-resolution simulation is conducted with three nested domains having a horizontal resolution of 18, 6, and 2 km with the 35 vertical levels in the advanced research WRF (WRF-ARW) model. The sensitivity experiment is carried out with seven planetary boundary layer (PBL) schemes; non-local first-order closure [Yonsei University (YSU), Asymmetric convective model, version 2 (ACM2), and Shin-Hong], local one-and-a-half order [Mellor–Yamada–Janjic (MYJ), quasi-normal scale elimination (QNSE), Bougeault–Lacarrère (BouLac), and Grenier–Bretherton–McCaa (GBM)] and five microphysics (MP) schemes [WSM6, Goddard, WDM6, Thompson, and Lin et al.]. PBL parameterization in combination with the Lin et al. scheme shows a significant impact on rainfall and dynamical and thermodynamical parameters at the surface and the upper levels. QNSE showed a relatively deeper and warmer atmospheric boundary layer compared to others to support strong upper-level divergence and high moisture content within the lower levels. Based on the results, QNSE is found to have a relatively better skill for representing the conducive environment, and Lin et al. microphysics could accommodate the same for the occurrence of the intense monsoonal rainfall events over Mumbai. The said combination is possibly effective for other coastal areas of India for better prediction of intense monsoonal rainfall episodes as well.

**Keywords:** WRF, PBL, TKE, rainfall, microphysics.

## 1. Introduction

The atmospheric boundary layer (ABL) is the lowest part of the atmosphere (up to 3 km) within the troposphere and is characterized by friction and turbulent mixing (Garratt, 1994; Stull, 1988). It is governed by the heat and momentum fluxes, buoyancy, wind shear, and turbulence due to a strong interaction with the underlying ground surface. It responds to the surface forcing within a time scale of about an hour or less (Stull, 2012). The ABL plays a vital role in the transportation of mass and energy (including momentum, heat, and moisture) into the upper part of the troposphere, which acts as a feedback mechanism for wind circulation. Therefore, boundary-layer processes are essential in the evolution of the lower atmospheric fields and other state parameters. The depth and structure of the ABL are determined by the physical and thermal properties of the underlying surface, along with the dynamics and thermodynamics of the lower atmosphere (Boadh et al., 2016). In numerical weather prediction, the complex processes of the ABL are resolved using the planetary boundary layer (PBL) parameterization schemes, which are developed considering the diurnal variability of the parameters (Moeng, 1984).

PBL parameterizations, in combination with appropriate surface layer schemes, are found to be highly sensitive for the precipitation simulation over Seoul (Shin & Hong, 2011). PBL parameterization directly impacts the vertical mixing and modulates the mixed layer depth along with associated moisture availability (Sathyanadh et al., 2017). High vertical mixing transports more moisture from the surface to the free atmosphere and favors the precipitation associated with the heavy rainfall events (Wisse &

---

**Supplementary Information** The online version contains supplementary material available at <https://doi.org/10.1007/s00024-021-02813-z>.

---

<sup>1</sup> Department of Earth and Atmospheric Sciences, National Institute of Technology Rourkela, Dist: Sundargarh, Rourkela, Odisha 769008, India. E-mail: pandaj@nitrkl.ac.in; jagabandhu@gmail.com

Arellano, 2004). In contrast, the weak vertical mixing confines moisture to the lower levels, which decreases the condensates and corresponding latent heating, hence reducing the surface precipitation (Efstathiou et al., 2013). Both local and non-local approaches can parameterize the vertical mixing processes. The non-local one substantially improves the precipitation forecast by enhancing the convective overturning (Hong & Pan, 1996). However, the local schemes are not expected to behave correctly under a fully developed turbulence scenario (Stull, 1991). Nonetheless, they can still compete with non-local schemes by adding higher-order terms. Previous works show local schemes tend to produce unrealistic shallow and moist boundary layers (Alapaty et al., 1997; Bright & Mullen, 2002; Hong & Lim, 2006; Stensrud & Weiss, 2002) due to their inability to represent large-scale turbulence and the underestimation of entrainment. The non-local schemes are not always skillful (Deng & Stauffer, 2006) and may produce deeper boundary layers in the windy conditions (Braun & Tao, 2000; Persson et al., 2001).

Besides the PBL, cloud development and associated physical processes within the boundary layer are also governed by other physical parameterization schemes (viz. microphysics or convection). Few studies have suggested that the rainfall forecast by a numerical model is more sensitive for the PBL and microphysics schemes than land surface models (Singh et al., 2018). For instance, Srinivas et al. (2018), using the weather research and forecasting (WRF) model, showed the impact of PBL parameterizations during an extremely heavy rainfall event while analyzing the associated physical processes, including the modulation of the upper air circulation, energy transport, moisture convergence, and intensity of convection. Microphysics parameterization is fundamental for the development, amount, and type of cloud (Liu and Avissar, 1996). Rajeevan et al. (2010) found underestimation of convection strength and vertical growth of the storm using all popular microphysics parameterizations and multiple observational platforms over the Indian region, and they advocated the need for their improvement. The irregularities in vertical cloud buildup and the up/downdraft can produce a higher or lower amount of precipitation. The choice of microphysics

scheme can significantly affect the rainfall statistics irrespective of the temporal scale of the simulation (Orr et al., 2017; Pieri et al., 2015). Microphysics parameterization also helps differentiate between cold and warm rain processes to appropriately reproduce the cloud physical parameters depending upon the geography and altitude of the location (Hong et al., 2010; Orr et al., 2017). Recently, Rath and Panda (2020) also showed the impact of microphysical parameterizations on WRF-simulated rainfall during convectively driven rain events over an urban area. They advocated using the 'Lin et al.' microphysical parameterization to better represent mixed-phase cloud processes within the WRF modeling framework while simulating convectively driven rain events.

Although some studies highlighted the significance of PBL and others the microphysics schemes, very few took them together to signify their role during monsoonal heavy rainfall scenarios. Thus, the main objective of this work is to highlight the sensitivity of the PBL and microphysics schemes during monsoonal heavy rainfall events over Mumbai, India, using the advanced research WRF model. Turbulence kinetic energy (TKE, one-and-a-half order local closer) and non-TKE (first-order non-local closer) schemes are compared in the present study. Several studies of sensitivity to PBL schemes have been carried out with the WRF model and its predecessor MM5 (Bright & Mullen, 2002; Zhang & Zheng, 2004; Deng & Stauffer, 2006; Hong & Lim, 2006; Weisman et al., 2008; Shin & Hong, 2011). Most of them focused on short periods of a few days or weeks and relatively smaller domains with flat and homogeneous topography (Stensrud, 2009). However, we explicitly identify the impact of seven PBL parameterization schemes in the WRF model for the simulation of heavy to very heavy rainfall (> 100 mm) events over Mumbai. Details about the data and methodology, including brief reviews of PBL and microphysical schemes, are presented in Sect. 2. The WRF simulated results are discussed in Sect. 3, which is followed by summaries of the findings in the last section.

2. Study Area, Data, and Methodology

During the active phase of the southwest monsoon (June–September), the regions windward to the Western Ghats (a north–south mountain range in western India), like Mumbai, Konkan, Goa, and Karnataka, gets heavy rainfall because of the orographic effect. The present study focuses on the Mumbai region confined within 72° 40' E–73° 34' E longitude and 18° 31' N–19° 38' N latitude (Fig. 1). Besides the Arabian Sea on the western side, Mumbai hosts several lakes and some mountainous regions, mainly on the northern and eastern sides of the city. Mumbai reportedly receives more than 200 mm/day rainfall in several instances during the southwest monsoon season. Accordingly, the heavy rainfall events with > 100 mm/day of precipitation are identified during 2014–2018 based on the reports of the India Meteorological Department (IMD) (<http://imd.gov.in/section/nhac/termglossary.pdf>). This study considered 30 heavy rainfall cases for performing simulations using the WRF model. Out of these, 16 cases (Table 1) are finalized based on the

Table 1

Detailed information of selected events based on the IMD report

Years	Start date	Rainfall (mm day <sup>-1</sup> )
2014	02-July	207
	09-July	112
	15-July	228
	27-July	144
2015	19-Jun	190
	2016	
2016	20-Jun	110
	28-Jun	105
	29-July	115
	05-Aug	143
	26-Aug	107
2017	28-Aug	153
2018	09-Jun	165
	23-Jun	152
	24-Jun	232
	02-July	131
	07-July	131

WRF output (model details described in Sect. 2.2) for further analysis discarding the rest. For choosing these 16 cases, three criteria were adopted similar to the study of Rath and Panda (2020), i.e. (i) amount

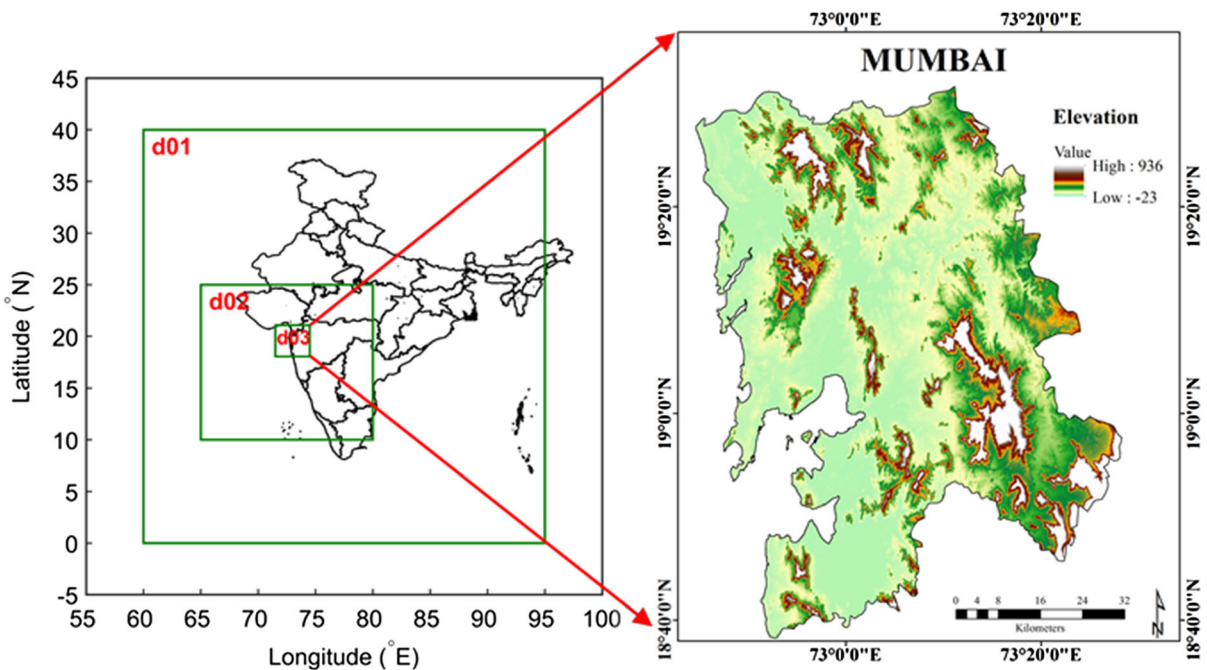


Figure 1 Domains used in ARW model simulations and elevation map of inner domain showing Mumbai city area

(observed rainfall > 100 mm/day; considered as a primary criterion) and duration of rainfall occurrence, (ii) similar time of onset (in both observation and model simulation) of rainfall on each day, and (iii) similar temporal and spatial trend (from model simulation) as that of the observations.

### 2.1. Data Used

For rainfall, global precipitation measurement mission (GPM-IMERG) data (<https://gpm.nasa.gov/data/directory>) with  $0.1^\circ \times 0.1^\circ$  horizontal resolution and 30-min temporal resolution was used to validate model simulations. The fifth generation of the European Center for Medium-Range Weather Forecasting (ECMWF) reanalysis ERA5 data set (<https://www.ecmwf.int/en/forecasts/datasets/reanalysis-datasets/era5>) was used for validation of the WRF model-derived meteorological parameters. The ERA5 data comes with a 31 km grid resolution on an hourly basis and resolves the atmosphere using 137 levels from the surface to the height up to 80 km. The ERA5 data is interpolated to match the horizontal resolution of the domain considered for WRF simulations. The reasons for using ERA5 data for comparison purposes include reasonable spatial and temporal resolution, data availability irrespective of the type of weather, and accuracy. The ERA5 data is only used where observations are not available. However, the observations for the near-surface variables, i.e., 2-m temperature, 10-m wind speed, and 2-m relative humidity, are taken from weather underground (<https://www.wunderground.com/>). For the vertical profiles of relative humidity, temperature, wind speed, and equivalent potential temperature, the data is considered from the Wyoming weather web (<http://weather.uwyo.edu/upperair/>) archive. Notably, several previous studies across the world (e.g., Srinivas et al., 2020; Tarek et al., 2020; Wang et al., 2020) and for various Indian megacities, including Mumbai, Delhi, etc., considered ERA5 in addition to meteorological observations for comparison with fine-resolution simulations at urban scale (e.g., Kumar et al., 2008; Rai & Pattnaik, 2019; Gunwani & Mohan, 2017).

### 2.2. Model Description

Advanced research WRF model version 3 (release 3.8.1) is adopted to carry out the numerical simulations. WRF is a fully compressible and non-hydrostatic next-generation mesoscale model with multiple nesting capabilities (Skamarock & Klemp, 1992; Wang et al., 2004; Skamarock et al., 2005). The model configuration consists of interactive three nested domains with the model top at 100 hPa. The horizontal resolution of the domains is 18, 6, and 2 km with 35 vertical levels, as shown in Fig. 1. The simulations are performed using the initial and boundary conditions, such as large-scale upper- and lower-layer circulation, moisture contents, and the thermal structures from the NCEP/NCAR FNL global 1-degree analyses. The MODIS (Moderate Resolution Imaging Spectroradiometer) land use was considered while performing the WRF simulations. For the innermost domain, 30-s land-use data from MODIS was used. Other land-surface-related information considered in the model input is the default information. Detailed information about the model configuration and experiment design can be found in Table 2. The experiments designed using different

Table 2  
Domain configuration used in the WRF model

Dynamics	Non-hydrostatics
Simulation duration	30 h
Initial conditions	6 hourly NCEP FNL ( $1^\circ \times 1^\circ$ ) data
Resolution	D01: $18 \times 18$ km, D02: $6 \times 6$ km, D03: $2 \times 2$ km
Grid points	$200 \times 247$ ; $256 \times 268$ ; $151 \times 163$
Vertical levels	35 terrain-following
Horizontal grid system	Arakawa-C grid
Integration time step	90 s
Time integration scheme	3rd order Runge-Kutta scheme
Spatial differencing scheme	6th order center differencing
Land surface parameterization	Noah land surface scheme
Microphysics	Lin et al. scheme
Shortwave radiation	Dudhia scheme
Longwave radiation	RRTM
Cumulus parameterization	Kain-Fritsch scheme

PBL and microphysical schemes besides surface physics are illustrated in Table 3. Other physics options in the WRF model, like longwave and shortwave radiation, cumulus, surface layer, and land surface parameterization, are selected based on available literature (Dawn & Satyanarayana, 2020; Kumar et al., 2008; Li et al., 2013, 2016; Panda & Sharan, 2012; Panda et al., 2009; Rajeevan et al., 2010; Rath & Panda, 2019, 2020). The selection of the particular set of PBL and microphysics schemes is primarily based on the view of conducting the urban specific simulations, type of physical processes and parameterizations considered in the available literature, and previous experience. Also, the parameterizations adopted in this study are based on their consideration of moisture processes and tendencies (cloud, rain, ice, snow, and graupel) so that the outcome can be well compared. However, the PBL and microphysical parameterizations are deliberated briefly here in line with the defined objective.

### 2.2.1 Brief Description of PBL Parameterization Schemes

In the PBL parameterizations, the sub-grid scale turbulent fluxes are parameterized using mean

prognostic variables such as surface exchange coefficient ( $c$ ), zonal ( $u$ ) and meridional ( $v$ ) wind, potential temperature ( $\theta$ ), and water vapor mixing ratio ( $q$ ), through vertical diffusion equations (Shin & Hong, 2011). The simplest form of vertical diffusion can be expressed as Eq. (1):

$$\frac{\partial C}{\partial t} = -\frac{\partial(\overline{w'c'})}{\partial z} = \frac{\partial}{\partial z} \left[ K_c \left( \frac{\partial C}{\partial z} \right) \right]. \quad (1)$$

Here,  $K_c$  is the diffusivity for the mean variable  $c$ .

In this current study, seven PBL schemes are used, which primarily follow two different approaches to compute the vertical transport of momentum, heat, and moisture. Among these PBL schemes, YSU (Hong & Lim, 2006), ACM2 (Pleim, 2007), and Shin-Hong (Shin & Hong, 2015) are classified as non-local first-order closure. These schemes are based on the  $K$ -theory (Stull, 1988), and they do not require any additional prognostic equations to express the effects of turbulence on mean variables. The  $K$ -theory follows a specific profile of the eddy diffusivity coefficient, which is a function of PBL height (PBLH), surface friction velocity, and stability. In the free atmosphere, the eddy diffusivity coefficient ( $K_c$ ) is a function of local wind shear and local Richardson number (Shin & Hong, 2011). The YSU scheme expresses the non-local mixing by simply adding a non-local gradient adjustment term ( $\gamma_c$ ) to the local gradient of each mean prognostic variable for heat and momentum. The diffusion equation for the prognostic variables are expressed as:

$$\frac{\partial C}{\partial t} = \frac{\partial}{\partial z} \left[ K_c \left( \frac{\partial C}{\partial z} - \gamma_c \right) - (\overline{w'c'})_h \left( \frac{z}{h} \right)^3 \right], \quad (2)$$

$$\gamma_c = b \frac{(\overline{w'c'})_0}{w_s h}. \quad (3)$$

Here,  $(\overline{w'c'})_0$  is the surface flux for the prognostic variables, and  $b$  is the proportionality constant. In Eq. (2), the second term on the right side is the entrainment flux proportional to the surface buoyancy flux (Srinivas et al., 2018).

The MYJ (Janjic, 1994), QNSE (Sukoriansky et al., 2005), BouLac (Bougeault & Lacarrere, 1989), and GBM (Grenier & Bretherton, 2001) schemes are classified as a local one and half order closer. These

Table 3

Details about the PBL schemes with the combination of relevant surface physics

PBL	Prognostic variable	Surface physics	Microphysics scheme
YSU	Non-TKE	MM5 similarity	Lin et al.
ACM2		MM5 similarity	
Shin-Hong		MM5 similarity	
MYJ	TKE	Eta similarity	
QNSE		QNSE similarity	Lin et al. WSM 6 Goddard WDM 6 Thompson
BouLac		MM5 similarity	Lin et al.
GBM		MM5 similarity	

schemes use turbulence kinetic energy (TKE) to parameterize eddy diffusivity through a mixing length approach. The eddy diffusivity coefficient for the heat and momentum that are parameterized in terms of TKE is defined as:

$$K_c = l\sqrt{e}S_c. \quad (4)$$

Here,  $S_c$  is the proportionality constant,  $l$  is the mixing length, and  $e$  is the TKE. Local closure schemes differ in consideration of  $S_c$  and  $l$  and apply the local mixing with the local diffusivity in Eq. (4) from the lowest to the highest vertical level for both convective boundary layer (CBL) and stable boundary layer (SBL).

These four parameterizations (MYJ, QNSE, BouLac, and GBM) are explained in more detail in Janjić (1990), Sukoriansky et al. (2005), Bougeault and Lacarrère (1989), and Grenier and Bretherton (2001), respectively. Notably, the QNSE PBL scheme uses the diffusivity term from the spectral theory to reflect the effects of internal wave generation in the presence of turbulence in a stably stratified boundary layer. The vertical scalar mixing is suppressed by the stable stratification, whereas vertical momentum mixing continues even at low Froude numbers (Sukoriansky et al., 2005). The QNSE theory is valid for stable stratification and weak unstable conditions (Galperin & Sukoriansky, 2010).

These PBL schemes are one-dimensional in higher grid scales and assume a clear scale separation between sub-grid and resolvable eddies. Boundary layer eddies start to resolve a fully three-dimensional local sub-grid turbulence scheme when the grid scale is within a few hundred meters (Skamarock et al., 2008). The surface layer physics determines friction velocities and exchange coefficients, which help compute surface heat and moisture fluxes by the land-surface parameterization and surface stress by the PBL scheme (Skamarock et al., 2008). The surface layer scheme also provides relevant stability information for use in the land surface and PBL parameterizations. Some PBL schemes like YSU require surface layer depth for representing the same within the model framework. And the PBL scheme could be coupled with an appropriate surface layer scheme (almost fixed) to determine the whole

atmospheric column behavior starting from the surface in a defined grid (Skamarock et al., 2008; Wang et al., 2017). For instance, the YSU, Shin-Hong, and GBM PBL schemes are only compatible with the MM5 similarity surface layer scheme (Wang et al., 2017). However, ACM2 and BouLac PBL parameterizations can also be used with PX and Eta similarity surface layer schemes, respectively, besides MM5 (Skamarock et al., 2008; Wang et al., 2017). The MYJ and QNSE PBL parameterizations can only be paired with the Eta similarity and QNSE surface layer schemes, respectively (Wang et al., 2017). Accordingly, the combinations for the considered PBL and surface layer physics are decided in the present study.

### 2.2.2 Brief Description of Microphysical Parameterization Schemes

A microphysical parameterization is a prerequisite for explicit representation and determination of water vapor, clouds, and precipitation-related processes in the modeling framework. The mass mixing ratios of cloud liquid water, cloud ice, snow, rain, and graupel are usually considered through the microphysical parameterizations, and in the WRF model, microphysics is carried out at the end of each time step as an adjustment process, and thus does not provide tendencies (Skamarock et al., 2008). The microphysical parameterizations in the WRF model include the sedimentation process and saturation adjustment, and the modeling framework allows the condensation adjustment. The microphysical parameterizations consider either bulk or bin representation. They may take into consideration ice-phase and/or mixed-phase processes. Accordingly, the spatial variability of rainfall and vertical variation of hydrometeors may vary.

Considering the type of microphysical parameterization, available literature, and previous experience (Dawn & Satyanarayana, 2020; Kumar et al., 2008; Rajeevan et al., 2010; Rath & Panda, 2020), five schemes, including Lin et al., Goddard, WSM6, WDM6, and Thomson, are used in this study. The Lin et al. scheme, based on Lin et al. (1983) and Rutledge and Hobbs (1984), is a single-moment scheme including modified saturation adjustment (Tao et al.,

1989) and ice sedimentation (Mitchell et al., 2008). It includes six classes of hydrometeors: water vapor, cloud water, rain, cloud ice, snow, and graupel. This scheme was one of the first to parameterize snow, graupel, and mixed-phase processes (such as the Bergeron process and hail growth by riming), and it has been widely used in numerical weather studies (Kumar et al., 2008; Rath & Panda, 2019, 2020).

Tao and Simpson (1993) introduced the Goddard microphysics scheme in WRF. This microphysical scheme has been modified to reduce the overestimated and unrealistic amount of graupel in the stratiform region (Tao et al., 2003; Lang et al., 2007). Also, saturation issues have been better addressed (Tao et al., 2003), and more realistic ice water contents have been obtained for long-term simulations (Zeng et al., 2008, 2009).

The WSM6 scheme has been developed by adding additional processes related to graupel to the WSM5 scheme. In this scheme, additional terms related to graupel are based on the reports of Lin et al. (1983) and Rutledge and Hobbs (1984). This scheme's prognostic water substance variables include the mixing ratios of water vapor, cloud water, cloud ice, snow, rain, and graupel. The WDM6 scheme (Lim & Hong, 2010) is the extended version of the WSM6 because it adds the prognostic number concentration of cloud and rainwater together with the cloud condensation nuclei (CCN); thus, prognostic water substance variables include water vapor,

cloud, rain, ice, snow, and graupel for both the WDM6 and WSM6 schemes.

The Lin et al. and WSM6 scheme parameterized the water vapor condensation into cloud liquid, cloud ice, rain, snow, and graupel. However, the Thompson et al. (2004) scheme carries an additional prognostic variable for the number concentration of cloud ice. According to Cooper (1986), primary ice nucleation is calculated, and the auto-conversion is considered similarly as that of Walko et al. (1995). A generalized gamma function represents the graupel category in the Thompson scheme instead of the exponential representation used in Lin et al. and WSM6 schemes.

Depending upon the meteorological scenario, one or more parameterizations may perform well based on a better representation of the physical processes involved. All the discussed microphysical parameterizations chosen for this study consider mixed-phase processes to resolve the updraft in a grid scale of 10 km or less, particularly in convective situations (Skamarock et al., 2008). The reason for considering such parameterizations is primarily to facilitate the city/urban scale simulation of convectively driven rain events and ease of comparison process.

### 2.3. Statistical Measures as Model Performance Indicators

Every statistical parameter plays a role in the validation of model performance and uncertainty

Table 4

Statistical measures used as model performance indicators

Statistics	Formulation
Bias	$\bar{P} - \bar{O}$
Standard deviation or SD ( $\sigma$ )	$\sqrt{1/N \left( \sum_{i=1}^N (M_i - \bar{M})^2 \right)}$
Normalized mean square error (NMSE)	$1/N \sum_{i=1}^N \frac{(P_i - O_i)^2}{P_i O_i}$
Index of agreement (IOA)	$1 - \frac{\sum_{i=1}^N (O_i - P_i)^2}{\sum_{i=1}^N ( P_i - \bar{O}  +  O_i - \bar{O} )^2}$
Root mean square error (RMSE)	$\sqrt{\frac{\sum_{i=1}^N (P_i - O_i)^2}{N}}$
Fractional bias (FB)	$\frac{\bar{O} - \bar{P}}{0.5(\bar{O} + \bar{P})}$

$P$  predicted value,  $O$  observed value,  $\bar{P}$  predicted mean value,  $\bar{O}$  observed mean value,  $M_i$  modeled value,  $\bar{M}$  modeled mean value;  $N$  sample size considered for computation

estimation, but some are considered more important (Borrego et al., 2008). In this study, model performance is evaluated using standard statistical parameters (Schlünzen & Sokhi, 2008; Emery, 2001; Gilliam et al., 2006) such as bias, standard deviation (SD), normalized mean square error (NMSE), index of agreement (IOA), root mean square error (RMSE), and fractional bias (FB). The mathematical formulations for bias, SD, NMSE, IOA, RMSE, and FB are given in Table 4. Bias measures the sign of the errors of the numerical simulations.

The positive values of the bias show the model over-predicts, and negative values show that the model under-predicts for a particular quantity. The SD is a measure of the spread of the individual modeled value from that of the mean. The NMSE is a measure of the overall deviations between predicted and observed values. The low NMSE value shows the model is performing well both in space and time; on the other hand, a high NMSE value does not mean

that the model is completely wrong. That could be due to shifting in time and space. IOA provides a measure of the match between the departure of each prediction and the departure of each observation from the observed mean (Willmott, 1981). IOA theoretically varies between 0 and 1, where 1 indicates the perfect match, and 0 indicates complete disagreement between observed and predicted values. RMSE measures the total model error between the predicted and observed values. FB is the normalized bias and varies from  $-2$  to  $2$ . A negative value of FB shows overestimation; however, positive values show underestimation by the model.

### 3. Results and Discussion

For evaluating the performance of each PBL scheme, the variation of some relevant variables considered, which includes temperature, relative

Table 5

Statistical performance indices for 2-m temperature ( $T_{2m}$ ), 10-m wind speed ( $WS_{10m}$ ), 2-m relative humidity ( $RH_{2m}$ ), and cumulative rainfall

Variable	PBL scheme	BIAS	SD	NMSE	IOA	RMSE	FB
$T_{2m}$ (°C)	YSU	-5.54	5.14	0.0028	0.115	5.56	0.232
	MYJ	-5.48	4.81	0.0027	0.118	5.49	0.229
	ACM2	-5.37	4.67	0.0026	0.115	5.39	0.224
	Shin-Hong	-5.36	3.98	0.0025	0.120	5.37	0.223
	QNSE	-5.06	5.21	0.0022	0.115	5.09	0.210
	BouLac	-5.12	3.93	0.0023	0.126	5.14	0.212
$WS_{10m}$ (m/s)	GBM	-5.36	3.98	0.0025	0.120	5.37	0.223
	YSU	2.39	2.22	0.0067	0.162	2.45	-0.50
	MYJ	2.85	3.13	0.0081	0.140	2.91	-0.57
	ACM2	2.29	1.88	0.0063	0.170	2.34	-0.48
	Shin-Hong	2.34	2.32	0.0065	0.163	2.40	-0.49
	QNSE	3.69	5.25	0.0107	0.099	3.77	-0.68
$RH_{2m}$ (%)	BouLac	2.28	2.11	0.0063	0.175	2.33	-0.48
	GBM	2.08	2.02	0.0057	0.182	2.14	-0.45
	YSU	-0.77	5.72	0.0000195	0.70	2.01	0.0084
	MYJ	-1.15	8.46	0.0000268	0.62	2.35	0.0126
	ACM2	-0.97	4.50	0.0000143	0.69	1.72	0.0106
	Shin-Hong	-0.96	6.17	0.0000212	0.65	2.10	0.0105
Cumulative rainfall (mm)	QNSE	-1.81	8.95	0.0000308	0.56	2.51	0.0198
	BouLac	-1.83	11.72	0.0000355	0.61	2.69	0.0201
	GBM	-1.15	7.11	0.0000243	0.60	2.24	0.0126
	YSU	-1.57	13.23	0.05	0.51	2.71	0.556
	MYJ	-1.86	14.33	0.07	0.50	2.87	0.694
	ACM2	-1.44	12.14	0.04	0.53	2.62	0.499
	Shin-Hong	-1.75	13.65	0.06	0.50	2.82	0.642
	QNSE	-0.75	10.31	0.02	0.42	2.52	0.231
	BouLac	-1.71	13.55	0.06	0.50	2.79	0.620
	GBM	-1.42	12.98	0.04	0.52	2.62	0.489



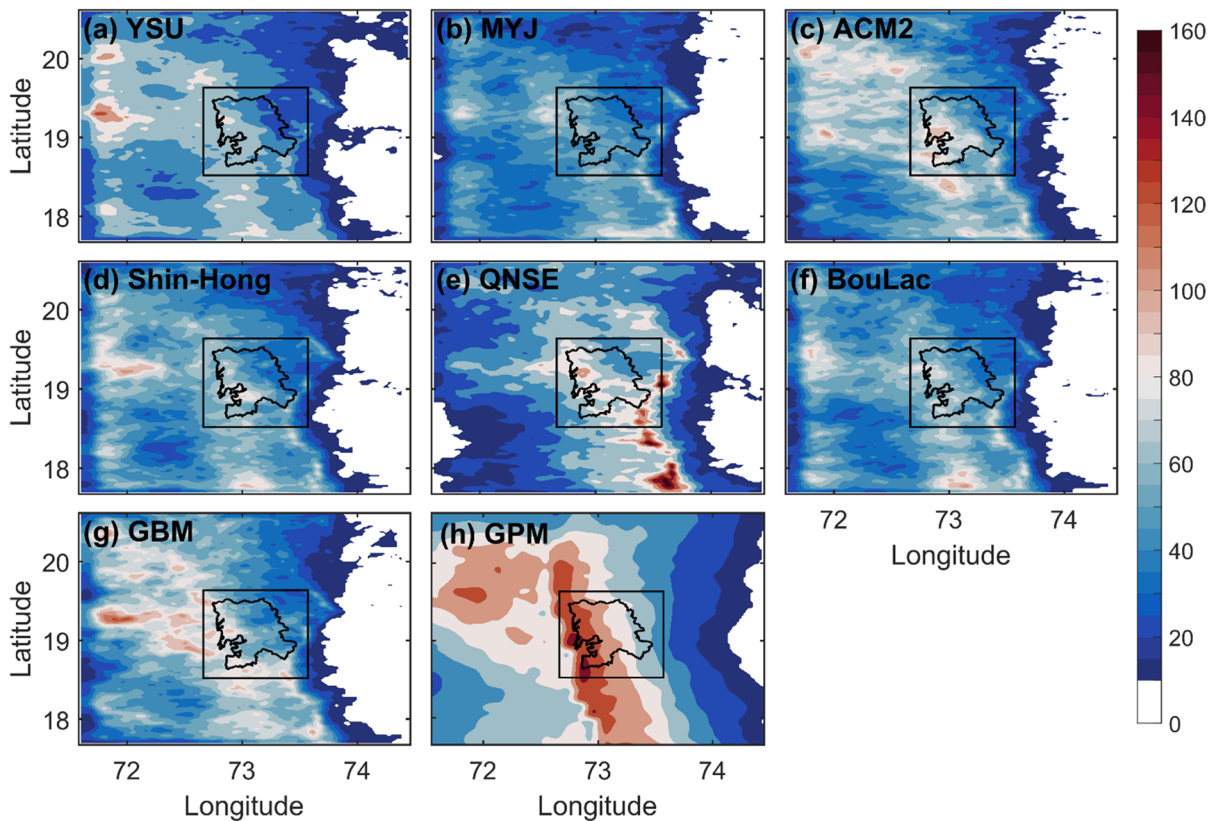


Figure 2

Spatial distribution of ensemble average accumulated rainfall (mm) over domain 3. The rectangular box within the domain shows the primary area of focus that encloses Mumbai city

humidity, wind speed, rainfall, surface fluxes, PBL height (PBLH), equivalent potential temperature, specific humidity, etc. A suitable and better PBL physics is considered for the selected WRF simulations to understand the sensitivity of rainfall predictability to microphysics. An ensemble approach similar to that of Li et al. (2013, 2016), Igri et al. (2018), and Rath and Panda (2019, 2020) is adopted for analyzing the simulated results. The model performance with seven PBL and five microphysical parameterization schemes at 2 km horizontal resolution compared with surface observations using different statistical measures is described in Sect. 2.3. And the statistical results are presented in Table 5.

### 3.1. Rainfall

Rainfall is one of the most important features of the summer monsoon season. Current analysis indicates the experiments could capture heavy rain pockets associated with the ensemble average but differ in spatial extent (Fig. 2). GPM observations indicate  $\sim 140$  mm of rainfall over western parts of Mumbai. The QNSE scheme shows rainfall distribution ( $\sim 160$  mm) over the east and southeast sides of the domain, whereas ACM2 and GBM show  $\sim 80$ – $100$  mm rainfall over the western side of the domain. It appears that the actual place of maximum rainfall has either shifted, or the model is redistributing the overall rain and under-predicting over certain locations. The rectangle box within domain 3 is the primary focused area where QNSE, ACM2, and GBM better capture the rainfall magnitude ( $> 90$  mm day $^{-1}$ ) than other experiments while

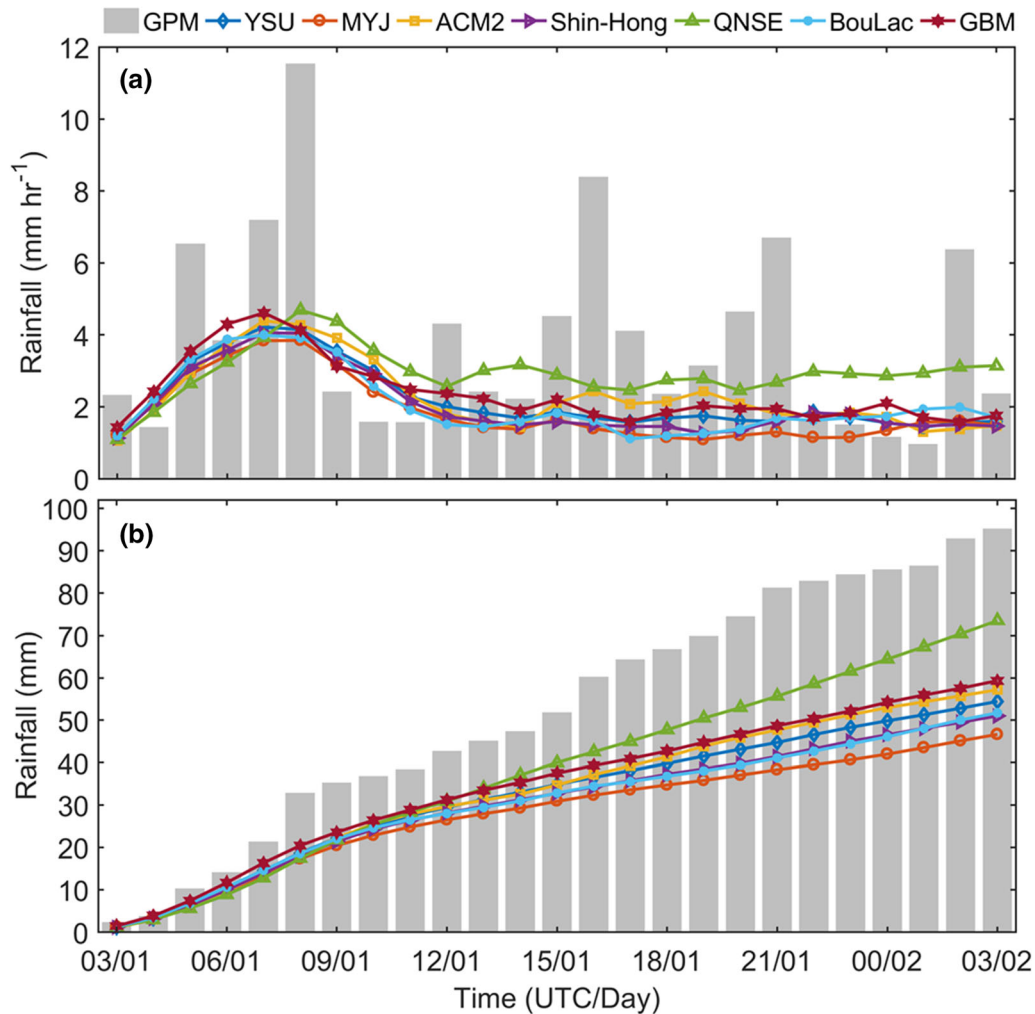


Figure 3

Time series of area-averaged **a** hourly rainfall ( $\text{mm h}^{-1}$ ) and **b** accumulated rainfall (mm) from all PBL experiments compared with GPM observations. The rectangular box shown in Fig. 2 is considered for area averaging of rainfall

comparing with GPM observations. The area-averaged rainfall (Fig. 3) shows that WRF simulations are unable to capture all the rainfall peaks. Time series of hourly rainfall (Fig. 3a) shows the experiment produces the highest rainfall peak ( $> 4 \text{ mm h}^{-1}$ ) at 07:00–08:00 UTC and the lowest simulated rainfall peak ( $< 2 \text{ mm h}^{-1}$ ) at 03:00 UTC of the first day. Most of the time, the hourly rainfall is less than  $4 \text{ mm h}^{-1}$  from 10:00 UTC onwards. And the experiment shows close resemblance from 03:00 to 05:00 UTC (also, during 13:00–14:00 UTC for cases other than QNSE), and after that, higher fluctuations

were noticed in the simulations. Some schemes like QNSE and GBM predicted the maximum ( $4.5\text{--}4.8 \text{ mm h}^{-1}$ ) and minimum ( $0.8\text{--}2.5 \text{ mm h}^{-1}$ ) rainfall than other TKE-based schemes. Among the non-TKE-based schemes, ACM2 predicted maximum ( $4\text{--}4.5 \text{ mm h}^{-1}$ ) and minimum ( $0.8\text{--}1.5 \text{ mm h}^{-1}$ ) rainfall than others. Accumulated rainfall (Fig. 3b) depicts that experiments are unable to capture the total rainfall. However, the QNSE follows a similar trend as GPM and predicted total rainfall of  $70\text{--}75 \text{ mm}$ , closer to the observations than the other PBL schemes. Overall, the model under-predicted the

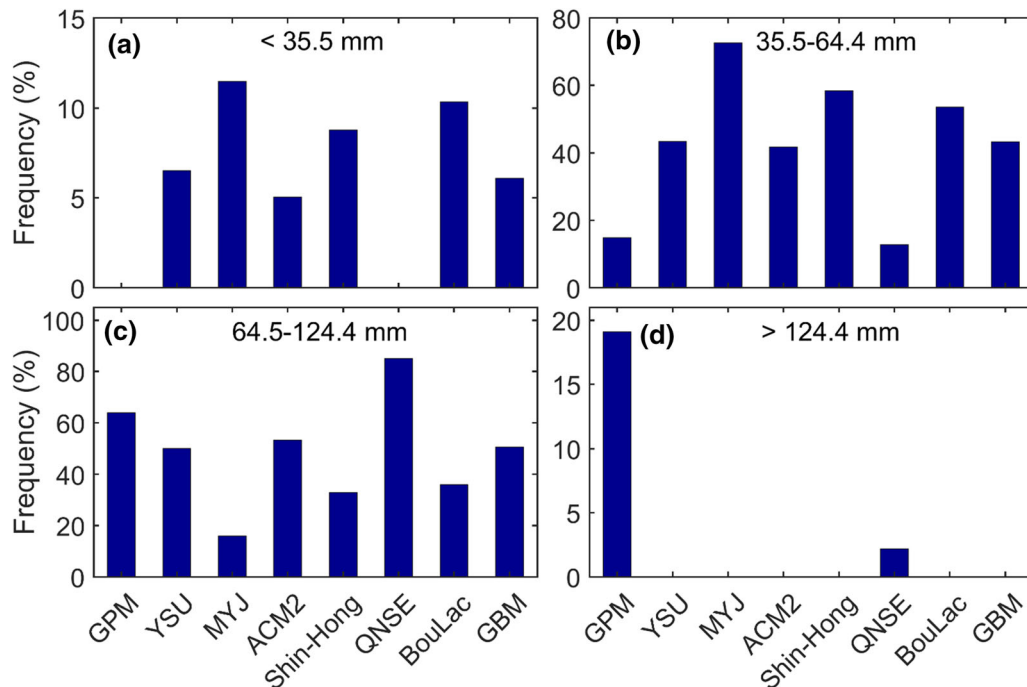


Figure 4

Frequency distribution of rainfall at different thresholds. Half hourly GPM data is used to validate the model simulated rainfall

rainfall for most of the time compared to the GPM observations, while the QNSE is performing relatively better than others in most instances (but for low rainfall, i.e.  $< 2 \text{ mm h}^{-1}$ , QNSE over-predicts, while other schemes performed somewhat better).

The statistical benchmarks for the model-simulated parameters shown in Table 5 should be  $\text{IOA} > 0.7$ ,  $\text{bias} = \pm 0.5$ , and  $\text{RMSE} = \pm 2$  (Emery, 2001). QNSE has a lower RMSE ( $= 2.53$ ) value than other schemes (Table 5). As compared to the GPM rainfall, ACM2 and GBM are closer to the QNSE with the RMSE value of 2.62. The magnitude of the bias, SD, NMSE, MSE, and FB was found to be relatively smaller for the rainfall prediction using the model with the QNSE PBL. The magnitude of IOA for rainfall is within the acceptable range ( $< 0.7$ ), with ACM2 showing better magnitude. Also, bias was found on the lower side ( $\text{bias} > -0.5$ ) of the acceptable range for rainfall, and QNSE shows comparatively less bias than others. Generally, for the rainfall, FB lies on the higher side of the acceptable range ( $\text{FB} > 0.5$ ) for YSU, MYJ, Shin-Hong, and BouLac, while for the ACM2, QNSE, and GBM,

it lies within ( $< 0.5$ ) the acceptable range (Table 5). Thus, the quantitative analysis based on statistical parameters considered here indicated that QNSE shows a better performance for the rainfall prediction by WRF (Fig. 3).

Figure 4 shows the frequency distribution of rainfall at different thresholds (low, moderate, heavy, very heavy) by considering the intensity-based categorizations by IMD. All the PBL schemes simulate higher rainfall (over-predict) at a moderate range ( $35.5\text{--}64.4 \text{ mm day}^{-1}$ ) except QNSE, which resembles better with observation in terms of grid points (Fig. 4b). QNSE performs relatively better in heavy ( $64.5\text{--}124.4 \text{ mm day}^{-1}$ ) and very heavy ( $> 124 \text{ mm day}^{-1}$ ) rainfall range than others (Fig. 4c, d) as well. Because of this reason, the overall rainfall is better predicted by WRF using QNSE. The consistency (inconsistency) in the model-simulated rainfall could be because of the appropriate (inappropriate) boundary layer response to the available atmospheric conditions to represent the convective scenario within the modeling framework. It could be associated with the relevant physical

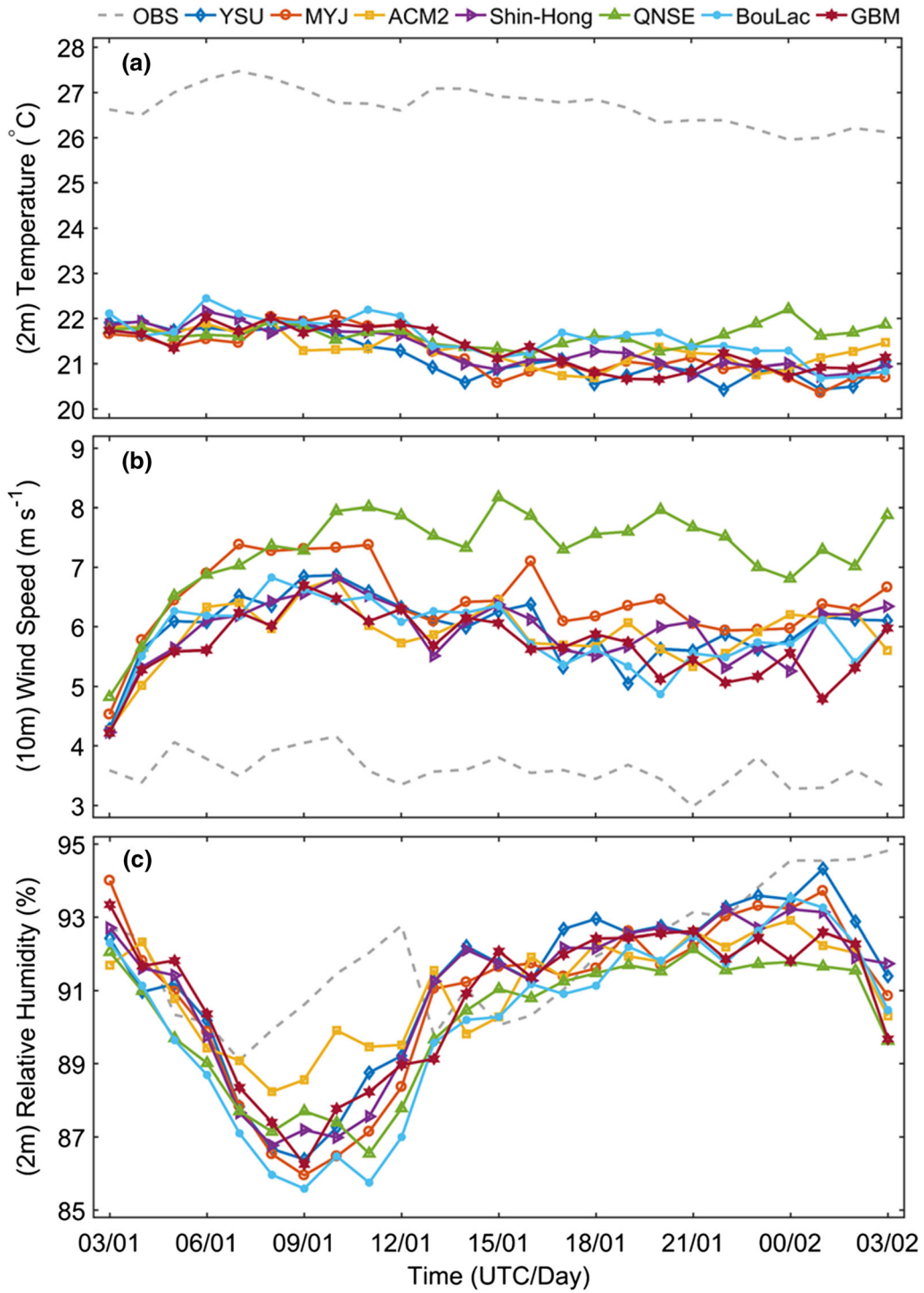


Figure 5

Time series of surface parameters a 2-m temperature, b 10-m wind speed, and c 2-m relative humidity compared with station observations

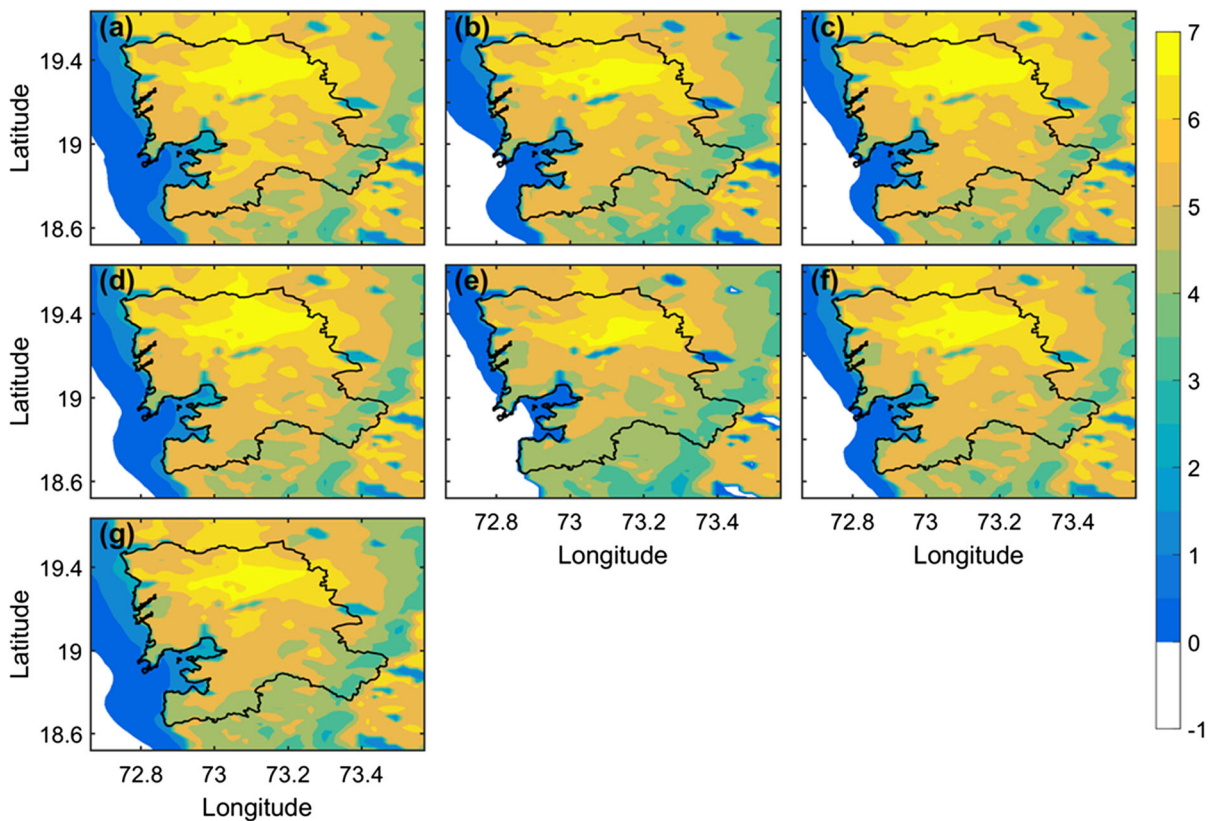


Figure 6

Spatial distribution of 2-m temperature difference ( $^{\circ}\text{C}$ ) of PBL experiments **a** YSU, **b** MYJ, **c** ACM2, **d** Shin-Hong, **e** QNSE, **f** BouLac, and **g** GBM from ERA5

processes and parameterization adopted for designing the concerned PBL scheme. The present study is probably the first of its kind to report a better performance of QNSE PBL parameterization for rainfall simulations in convective rain events during the summer monsoon period. The physical reasoning for better predictability of rainfall could be drawn from its actual behavior. The studies by Coniglio et al. (2013), Hariprasad et al. (2014), and Tastula et al. (2015) indicate that QNSE is capable of producing highly unstable conditions due to relatively higher CAPE and allows strong vertical mixing. Thus, it can support the formation of deep convective clouds and help produce higher intensity rainfall compared to other PBL parameterizations.

### 3.2. Near-Surface Basic Variables

The choice of PBL schemes substantially impacts the near-surface parameters like 2-m temperature ( $T_{2m}$ ), 10-m wind speed ( $WS_{10m}$ ), and 2-m relative humidity ( $RH_{2m}$ ). The comparison between the model simulations and station observations is illustrated in Fig. 5. The variation in the simulated values is similar when different PBL schemes are compared; however, the  $T_{2m}$  is underestimated while the model overestimates  $WS_{10m}$ . On the other hand,  $RH_{2m}$  is sometimes over-predicted and sometimes under-predicted. The diurnal variation of  $T_{2m}$  shows higher temperatures during 06–11 UTC, i.e., in the local afternoon (Fig. 5a). Inter-comparison did not show much variation during the whole period. The maximum deviation of  $0.5^{\circ}\text{C}$  is found among the experiments from 17 to 22 UTC during night time.

MYJ and GBM show similar variation throughout as the values mostly overlap.

The difference between the temperature from the model output (from the innermost domain) is presented in Figs. 6, S1, S2, and S3. The analysis by considering the maximum and minimum temperatures (Figure S1) indicates that the model results have less bias for the earlier ( $\sim 0.2$ – $1$  °C) than the latter ( $5.8$ – $6.3$  °C). The highest and lowest bias for maximum temperature was found for QNSE ( $\sim 1$  °C) and YSU ( $0.2$  °C), respectively. However, for the minimum temperature, QNSE simulated the lowest bias ( $5.7$  °C) while MYJ and BouLac show the highest bias ( $> 6$  °C). In the overall comparison, all the experiments were not able to simulate the minimum temperature accurately during the rainfall scenario. Spatial variation of the difference of simulated  $T_{2m}$  shows the highest bias (up to  $7$  °C) over the land and less over the ocean ( $-1$  to  $1$  °C) regions (Fig. 6). Here, the model predicted less temperature over most of the grid points over the land (Fig. 6), becoming the reason for the under-prediction of  $T_{2m}$  when compared with the observations (Fig. 5a). Separate day (Figure S2) and night (Figure S3) analysis for the spatial distribution of  $T_{2m}$  difference indicates higher bias during the earlier within the city boundary. In the northern part, bias is relatively higher as compared to the southern part of the city. The overall comparison indicates that the bias is minimal for the QNSE scheme for day and night-based analysis (Figures S2–S3). According to the WMO standards (Gordon & Shaykewich, 2000), the acceptable range of RMSE for temperature is  $\pm 2$  to  $\pm 3$  °C, and the acceptable range of the bias is  $\pm 0.4$  °C. In the present case,  $RMSE > 4$  °C and  $BIAS < -4$  °C (Table 5). However, most of the statistical indices suggest that the QNSE is performing better in predicting the near-surface air temperature. The larger errors realized in the present scenario may be attributed to the complex nature of the considered rain episodes and instrumental errors. Since the major focus is on rainfall in line with the current objectives, future studies may consider investigating such higher errors, which do not go well within the prescribed WMO standards.

The temporal variability of simulated  $WS_{10m}$  shows the highest peak ( $> 5$   $ms^{-1}$ ) during 06–12

UTC (local afternoon / late afternoon) of the day and the lowest peak at 13–24 UTC during night time (Fig. 5b). All the experiments overestimate  $WS_{10m}$ ; however, GBM could represent it better than others (Table 5), mainly during the night. During the day, ACM2 and GBM are both able to represent it better (Fig. 5b). And the variation in  $WS_{10m}$  for ACM2 is similar to GBM for most of the time. QNSE and MYJ predicted higher  $WS_{10m}$  ( $4.3$ – $5.8$   $ms^{-1}$ ) from 03 to 10 UTC; after that, QNSE simulated wind speed was found to be consistently higher ( $> 5.5$   $ms^{-1}$ ).

Figure 5c illustrates the diurnal variation of  $RH_{2m}$  with the highest value ( $\sim 95\%$ ) during nighttime or early morning hours and the lowest value ( $\sim 85\%$ ) during the daytime. Most of the time, the model prediction does not follow the observational trend. However, the variation in  $RH_{2m}$  between the experiments/simulations is nearly 2%.

The quantitative analysis for the predictability of near-surface parameters  $T_{2m}$ ,  $RH_{2m}$ , and  $WS_{10m}$  while evaluating the performances of PBL parameterizations is based on statistical parameters shown in Table 5. For  $T_{2m}$ , the QNSE shows less error with RMSE and NMSE values 5.09 and 0.0022. Based on the statistical indices, GBM and ACM2 perform relatively better in predicting  $WS_{10m}$  and  $RH_{2m}$ . However, the indices indicate that the performances of QNSE are not too bad in comparison to those of GBM and ACM2 for the corresponding parameters. Notably, the magnitudes of IOA for these three near-surface parameters are below the acceptable range for all PBL schemes (Table 5). Generally, for all near-surface parameters considered here,  $FB < 0.5$ , where positive FB is seen for  $T_{2m}$  and  $RH_{2m}$  and negative for  $WS_{10m}$  (Table 5). The statistical indices considered in this study indicate that none of the PBL schemes is consistent in its performance for simulating the near-surface variables  $T_{2m}$ ,  $WS_{10m}$ , and  $RH_{2m}$ .

In the surface layer, the basic near-surface variables considered here mostly depend upon the surface layer and vertical diffusion formulations (Shin & Hong, 2011) and, thus, modulated through different combinations of PBL and surface layer physics adopted. Some PBL parameterizations along with their compatible surface-layer scheme, tend to perform better in simulating near-surface basic

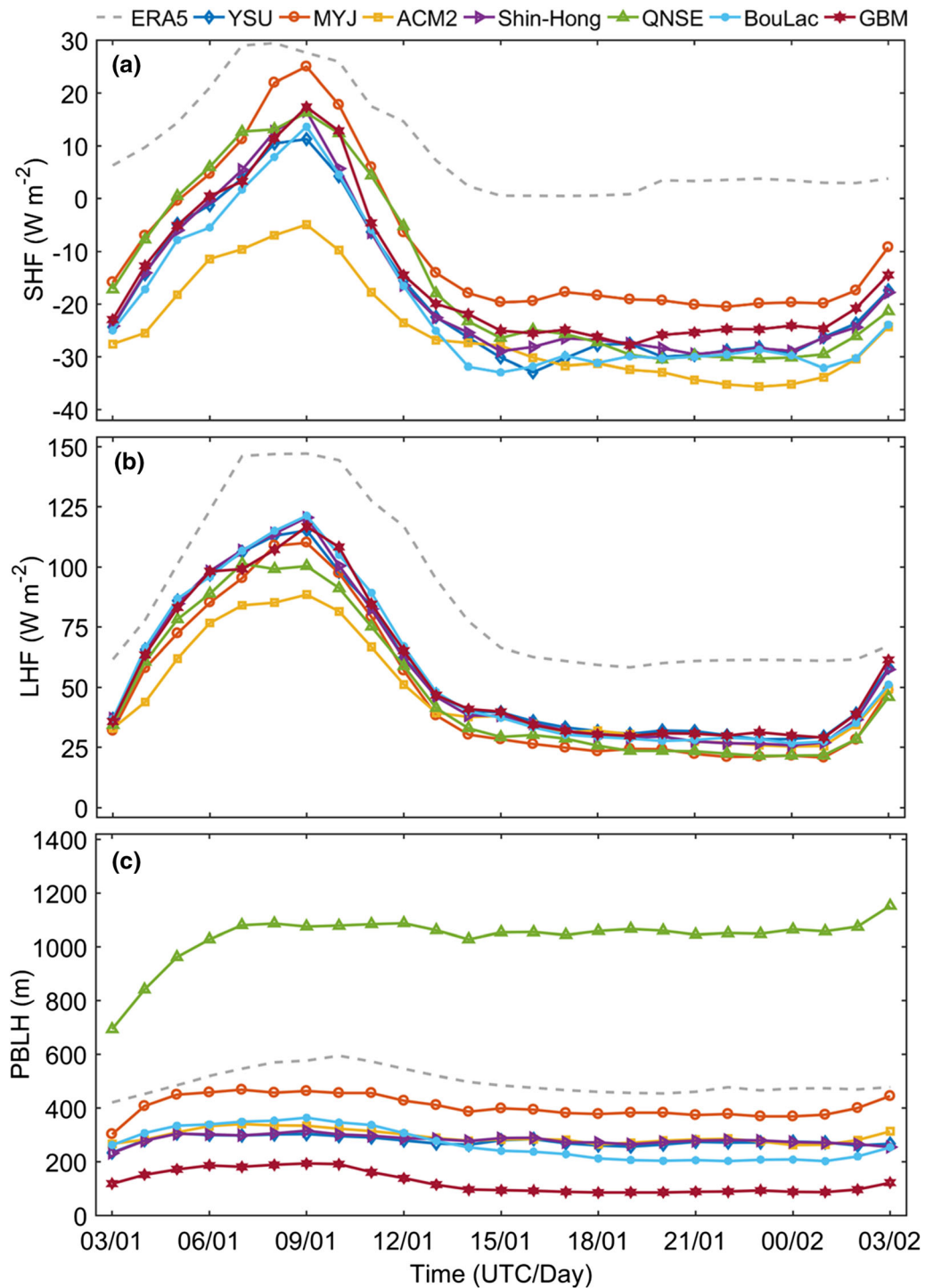


Figure 7

The diurnal variation of PBL parameters **a** sensible heat flux (SHF), **b** latent heat flux (LHF), and **c** planetary boundary layer height (PBLH) compared with ERA5

variables. Still, some others cannot work correctly due to the stability functions used and the methodology adopted to parameterize the associated processes. The studies by Tastula et al. (2015) and Coniglio et al. (2013) indicate that QNSE produces relatively higher kinetic energy at high wind speeds that amplify the eddy diffusivity and also yields high CAPE values resulting in a highly unstable and deep convective boundary layer within the modeling framework (Hariprasad et al., 2014). Thus, QNSE appears to be better equipped to represent the convective conditions like the present ones. Therefore, it may be able to predict the near-surface variables in a better manner compared to other PBL parameterizations. The same is true mainly for  $T_{2m}$  (Gunwani & Mohan, 2017). Thus, the qualitative and quantitative analysis indicated that QNSE shows a relatively better performance for  $T_{2m}$  (Fig. 5a) and shows a reasonable skill in simulating the variation of  $RH_{2m}$  (Fig. 5c) and  $WS_{10m}$  over Mumbai during the considered heavy rain events. However, further investigation is required to arrive at a concrete conclusion in this regard.

### 3.3. Surface Fluxes and PBL Height

For understanding the role of PBL parameterizations in governing the variability in the near-surface fluxes (sensible and latent heat) and planetary boundary layer height (PBLH), the temporal/diurnal variation of these parameters is analyzed. Figure 7 shows the diurnal variation of sensible heat flux (SHF), latent heat flux (LHF), and PBLH. An increasing trend in the surface fluxes is realized in the daytime with higher values from 06 to 10 UTC (mainly in the afternoon), and then the values start decreasing to achieve a minimum post-mid-night before the following day. During the nighttime, fluxes are very low; LHF is positive but less than  $50 \text{ Wm}^{-2}$  and SHF is negative but  $> -40 \text{ Wm}^{-2}$ . During the nighttime, the negative values of SHF indicate that the model produces a warmer, lower atmospheric layer than the land surface. The MYJ PBL simulates the highest magnitude ( $-17$  to  $26 \text{ Wm}^{-2}$ ) of the SHF, and ACM2 simulates the lowest ( $-5$  to  $-35 \text{ Wm}^{-2}$ ) when compared with the others (Fig. 7a). During the daytime, relatively higher LHF ( $> 100 \text{ Wm}^{-2}$ ) is

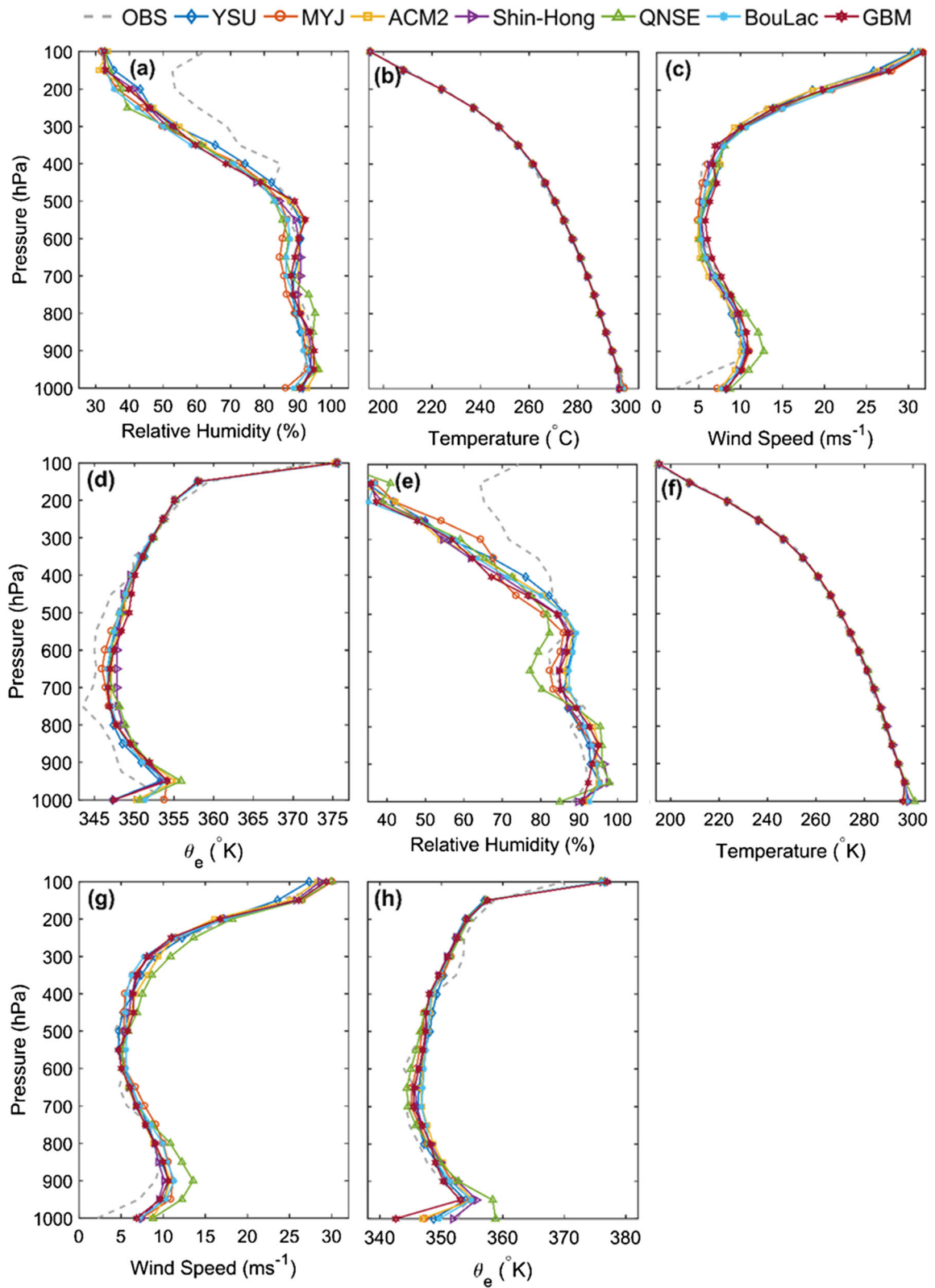
Figure 8

Validation of simulated mean vertical profile of relative humidity (%), temperature ( $^{\circ}\text{K}$ ), wind speed ( $\text{ms}^{-1}$ ), and equivalent potential temperature ( $^{\circ}\text{K}$ ) at 12:00 UTC on the same day (a–d) and at 00:00 UTC the next day (e–h). Here, the comparison is done with station observations

simulated by the model while using BouLac, which is coherent with the YSU and Shin-Hong, and the lower values are simulated when ACM2 ( $\sim 85 \text{ Wm}^{-2}$ ) adopted (Fig. 7b). All the experiments underestimate the SHF and LHF throughout the simulation period. Overall, inter-comparison among all the experiments indicates a difference of  $> 25 \text{ Wm}^{-2}$  between the maximum and  $15 \text{ Wm}^{-2}$  between the minimum SHF values. The corresponding differences for maximum and minimum values of LHF are  $> 30 \text{ Wm}^{-2}$  and  $< 15 \text{ Wm}^{-2}$ , respectively. The simulated diurnal/temporal variation of surface fluxes supports the usual presumption and is found to be physically consistent.

Figure 7c demonstrates the temporal variation of PBLH. Here, PBLH is higher during day time and lower during the night (e.g., 600 m during 06–12 UTC and 400–500 m during 13 UTC–03 UTC the next day according to ERA5). PBLH predicted by the MYJ is closer to the ERA5 than others, while the model simulation adopting QNSE over-predicted the same. The overall comparison indicates that all model simulations underestimate the PBLH except QNSE when the values are compared with those of ERA5. The over prediction of PBLH by QNSE may be linked with the higher convective available potential energy (CAPE) and deeper convective boundary layer consideration (Coniglio et al., 2013; Hariprasad et al., 2014). Also, ERA5, being a global data set, may not capture the localized effects appropriately. Nevertheless, the deeper or shallow PBLH could be associated with intense or weak moisture transport and consequent moist instability, which, in turn, may modulate the rainfall distribution (Rai & Pattnaik, 2019) as noticed in the current scenario. Although it is difficult to draw any conclusion regarding the PBLH predictability, qualitatively, QNSE with higher PBLH supports the hypothesis of greater moist





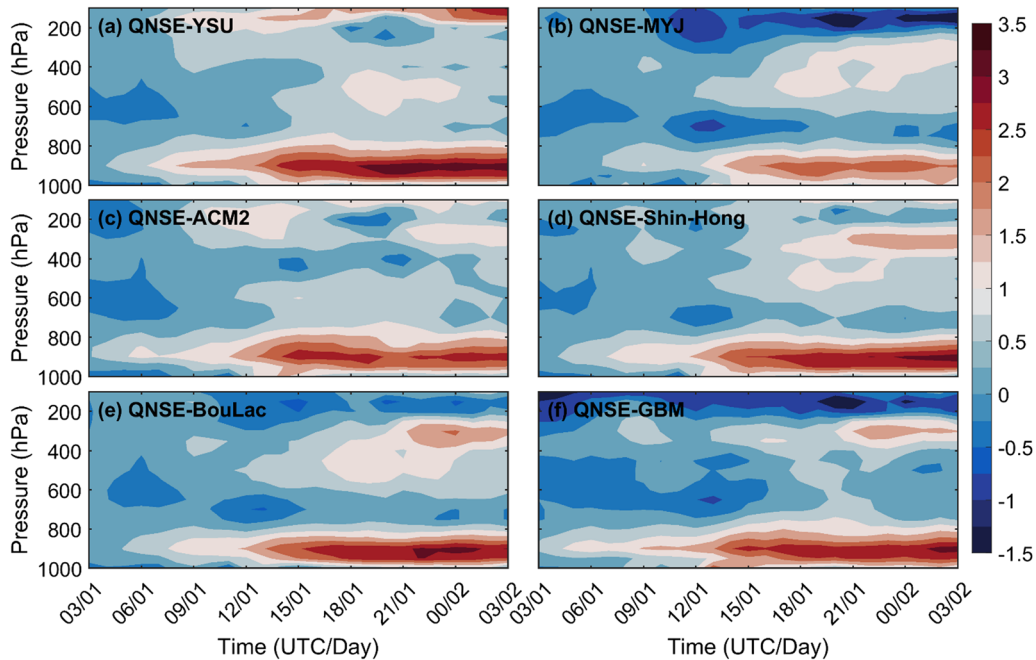


Figure 9

Time series plot of spatial mean differences in the vertical distribution of wind speed for **a** QNSE-YSU, **b** QNSE-MYJ, **c** QNSE-ACM2, **d** QNSE-Shin-Hong, **e** QNSE-BouLac, and **f** QNSE-GBM

instability, which is physically consistent with the convective condition during the rainfall scenarios.

### 3.4. Vertical Characteristics

The vertical variations of simulated relative humidity, temperature, wind speed, and equivalent potential temperature are compared with the available station observations at 12:00 UTC of the first day and 00:00 UTC of the next day as per the availability of data from the Wyoming weather web archive (Fig. 8). The comparison demonstrates that the model-simulated relative humidity is quite close to the observations between 1000 and 500 hPa and underestimates above it, but follows similar trends (Fig. 8a and e). The vertical profiles of the temperature and equivalent potential temperature follow similar trends as that of observations (Fig. 8b, d, f, and h). All the experiments show less variability near the surface for the air temperature and equivalent potential temperature. Figure 8c and g show the vertical profile of the wind speed, where the model was found to be over-predicting from the surface up

to 600 hPa. The model shows a wind maximum near 900 hPa above the boundary layer and is valid for all PBL parameterizations considered in this study (Fig. 8c and g), indicating the impact of land-atmosphere interaction. The qualitative inter-comparison of PBL schemes shows that QNSE has a reasonably better prediction skill than others. The reason for the improved predictability during the extreme weather condition could be better consideration of vertical diffusion and good representativeness of convective conditions within the modeling framework (Coniglio et al., 2013; Tastula et al., 2015). Therefore, for further comparison, QNSE is used as a benchmark, and other PBL schemes are evaluated against it.

Figure 9 shows the temporal variation of the difference of area-averaged wind speed between other experiments and the one using QNSE. The comparison shows wind speed has relatively less difference (about  $-0.5$  to  $1.5$   $\text{ms}^{-1}$ ) from the near-surface to 800 hPa during the initial 9 h of simulation, i.e., 03:00–12:00 UTC on the first day and after that, it is higher ( $> 1.5$   $\text{ms}^{-1}$ ). In the mid-troposphere

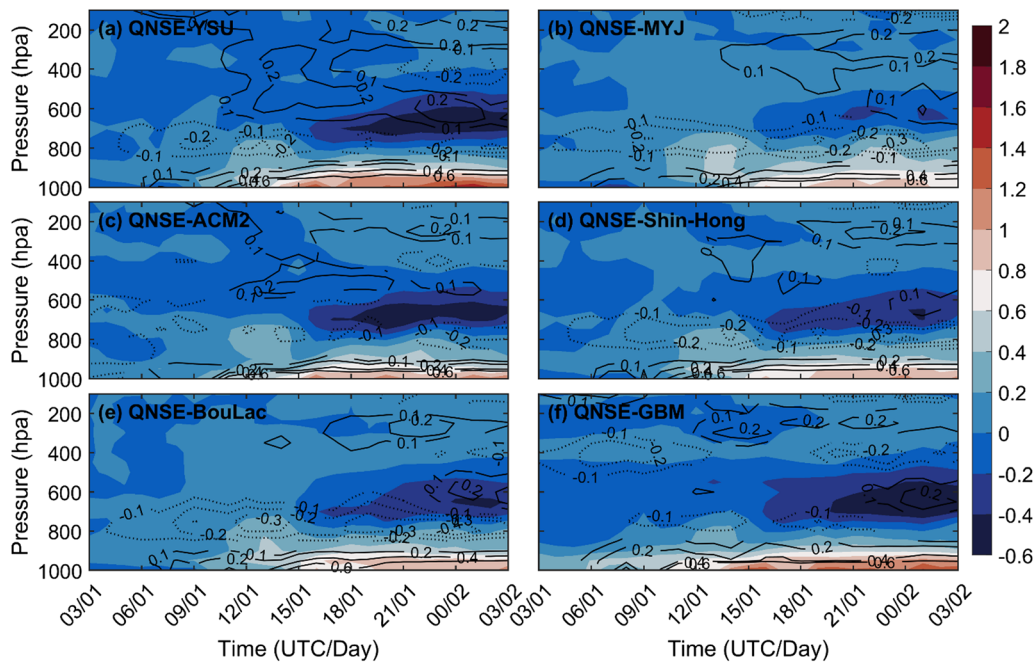


Figure 10

Time series plot for spatial mean differences in the vertical distribution of specific humidity (shaded;  $\text{g kg}^{-1}$ ) and temperature (contours;  $^{\circ}\text{C}$ ): a QNSE-YSU, b QNSE-MYJ, c QNSE-ACM2, d QNSE-Shin-Hong, e QNSE-BouLac, and f QNSE-GBM

region (800–600 hPa), wind differences are relatively less for MYJ, BouLac, and Shin-Hong schemes during the period from 12:00 UTC of the first day to 03:00 UTC of the next day. Higher wind difference from 12:00 UTC onwards shows an increase of wind shear in the lower troposphere for QNSE. The variation in wind speed directly affects the moisture availability, and the presence of moisture may also vary due to phase change, particularly in the middle troposphere, which modulates the temperature (Rai & Pattnaik, 2019). All experiments show an almost similar pattern within the lower troposphere for having weaker wind shear, which reduces the PBLH (Fig. 7c).

Figure 10 represents the pressure–time distribution of the difference of specific humidity (shaded) and temperature (contours) from different experiments with respect to QNSE. Here, positive and negative temperature values are represented by solid and dashed lines, respectively. The increase (decrease) in temperature in the region 850–400 hPa is associated with a decrease (increase) in specific humidity. For MYJ, BouLac, and Shin-Hong, the

variation in specific humidity above 850 hPa is qualitatively coherent with wind speed, and an increase to decrease in wind speed (Fig. 9) is associated with a decrease to increase in specific humidity (Fig. 10). Above 500 hPa, the specific humidity shows less variation ( $< 0.1 \text{ g kg}^{-1}$ ); however, the temperature is mostly lesser than the QNSE. Also, QNSE produces moist lower layers (1000–950 hPa) compared to others.

The pressure–time variation of spatial mean differences (with respect to ERA5) of wind speed ( $\text{ms}^{-1}$ ) was analyzed further for understanding the performance of various PBL parameterizations (Figure S4). The analysis indicates that the simulated horizontal wind speed is relatively higher within 800 hPa from the surface. It would eventually increase the wind shear giving rise to higher PBLH (Fig. 7c). Higher PBLH supports enhanced convection and eventually increasing moisture availability leading to higher humidity (Figs. 10 and S5). Therefore, QNSE strongly supports this hypothesis and can represent the prevailing convective conditions in a better manner.

Further, the pressure–latitude plots for longitudinally and temporally (05:00–10:00 UTC) averaged air temperature difference between the other experiments and QNSE are analyzed to investigate the warming within the lower layer (Figure S6). During this period, most of the rainfall occurred over 18.5–19.5 °N and 72.66–73.20 °E. Therefore, the longitudinal average (72.66–73.20 °E) is obtained during the time 05:00–10:00 UTC (10:30–15:30 local time). The simulations considering QNSE and MYJ parameterizations were found to be predicting relatively higher and lower rainfall (Fig. 3; Table 5) with the warmest lower layers for QNSE (Figs. 5a, S6) than others. Therefore, the higher rainfall occurrence is associated with a warmer temperature over the selected region. And warmer air temperature, especially over the northern and western side of the city (Sect. 3.2), is mainly associated with the intense convection in the case of QNSE, which is responsible for the higher rainfall predictability.

### 3.5. Impact of Microphysical Parameterizations

The QNSE PBL scheme is paired with different microphysics schemes for understanding the characteristic features associated with the microphysical parameters during the heavy rainfall scenarios over Mumbai. The ensemble-averaged time series of hourly and accumulated rainfall is analyzed for this purpose (Figure S7). The model has simulated the highest rainfall ( $\sim 4 \text{ mm h}^{-1}$ ) at 08:00 UTC (1:30 pm local time) and the lowest rainfall ( $< 1.5 \text{ mm h}^{-1}$ ) at 03:00 UTC, i.e., in the morning hours around 8:30 am local time. The highest peak of the rainfall is under-predicted by the model outputs as compared to the GPM observations. The magnitude of predicted total rainfall is  $< 75 \text{ mm}$ , while from

GPM, it is  $> 90 \text{ mm}$ . The inter-comparison among different microphysics simulations indicates that the Lin et al. scheme has better skills to predict the rainfall with the RMSE value of 2.52 (Table 6). In the overall analysis based on ensemble averages, it is found that the model is not able to capture the rainfall effectively.

Further, the analysis is focused on a single event that occurred on 26 August 2016 (107 mm rainfall). The selection of this event is based on the amount and spatial distribution of simulated rainfall. Figure 11 shows the spatial and temporal distribution of rainfall for the considered event. The spatial distribution indicates that the model could capture heavy rain pockets only but differ in spatial extent. WSM6, Lin et al., Goddard, and Thompson show the rainfall is over-predicted ( $> 120 \text{ mm}$ ) by the model at some grid points in the eastern and northwestern sides. In view of the spatial extent, the rainfall captured by GPM is  $< 100 \text{ mm}$ . And the area-average variation shows that the model could capture the rainfall till 20:00 UTC, and afterward, it is under-predicted. Here, Lin et al. performed better than other microphysical parameterizations and captured the rainfall of  $\sim 45 \text{ mm}$ , while GPM observed rainfall is  $> 60 \text{ mm}$ .

Figure 12 demonstrates the rain rate and vertically integrated moisture transport in the lower troposphere (from 1000 to 850 hPa) for 26 August 2016. The increasing trend of moisture transport is seen during the decreasing rain rate, whereas the decreasing trend is seen during the increasing rain rate. Although Goddard simulated relatively higher moisture transport ( $211 \text{ kg m}^{-1} \text{ s}^{-1}$ ) at 06:00 UTC, possibly due to higher vertical mixing, it significantly increased in the case of Lin et al., Thompson, WSM6 for later hours after 15:00 UTC.

Table 6

*Statistical performance indices for rainfall with respect to GPM*

	MP scheme	BIAS	SD	NMSE	IOA	RMSE	FB
Cumulative rainfall (mm)	WSM6	−1.45	14.54	0.056	0.440	2.85	0.47
	Goddard	−1.22	12.91	0.042	0.445	2.72	0.38
	WDM6	−1.41	14.75	0.053	0.443	2.85	0.45
	Thompson	−1.11	12.52	0.038	0.421	2.72	0.34
	Lin et al.	−0.75	10.31	0.020	0.420	2.52	0.23

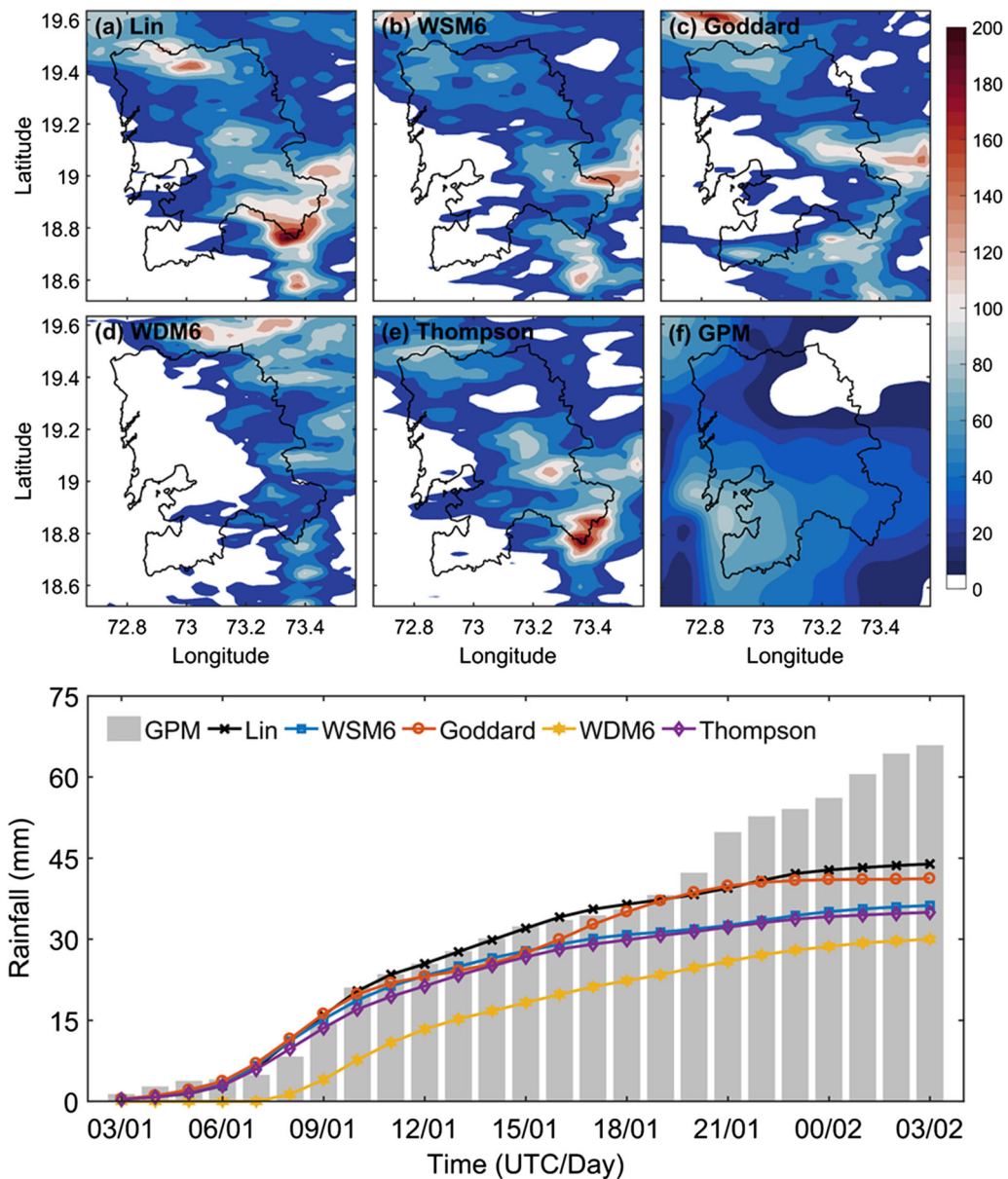


Figure 11  
 Spatial (above) and time series of area-averaged (below) accumulated rainfall for the 26 August 2016 case

The vertical variations of area-averaged water vapor mixing ratio, cloud water mixing ratio, and rainwater mixing ratio are analyzed (Fig. 13) to strengthen the understanding of the associated characteristic features and physical consistency. The water vapor mixing ratio is continuously decreasing with height, and at the surface, it is higher, but its value is appreciable till  $\sim 700$  hPa. It indicates the

presence of a significant amount of vertically transported moisture to support the formation of clouds in the atmosphere (Fig. 13a). There is a consistent increase in the area-averaged cloud water mixing ratio up to 700 hPa, which indicates the prevalence of low-level cumulus and stratocumulus cloud layer (Fig. 13b), supporting the occurrence of rainfall. Similarly, the vertical distribution of the rainwater

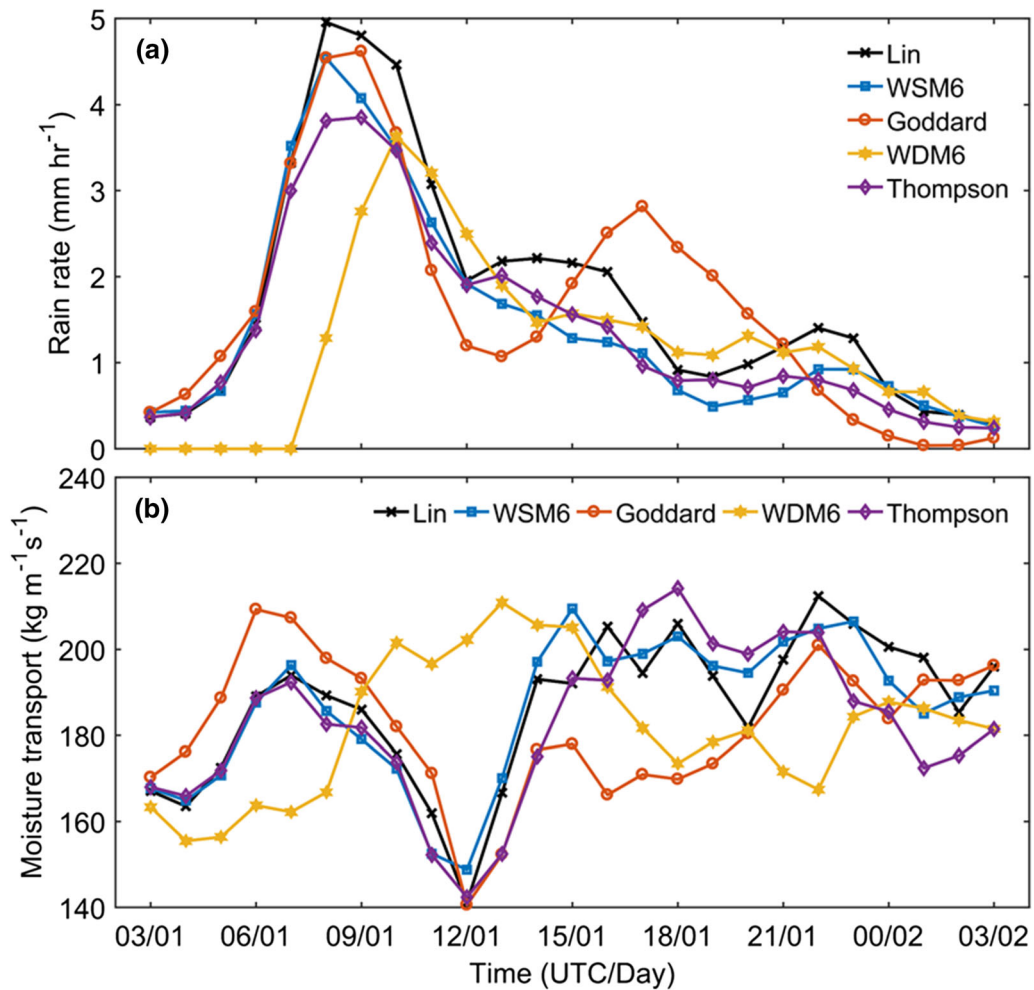


Figure 12

Temporal variation of **a** rain rate and **b** vertical moisture transport for different microphysical parameterization during the 26 August 2016 case

mixing ratio is affected by induced changes in cloud properties, i.e., the average rain mixing ratio generally increases, and raindrop number concentration decreases, implicating the diameter of raindrop would increase and enhance the chance of rain (Fig. 13c). The presence of a greater average rainwater mixing ratio is the indication of the development of deeper clouds with a greater amount of water content.

Figure 14 illustrates the temporal variation of domain average water vapor mixing ratio, cloud water mixing ratio, and rainwater mixing ratio at 850 hPa. Water vapor and cloud mixing ratios are relatively less during the highest rain rate scenario

(Fig. 12a). The highest peak of water vapor and cloud water mixing ratio was observed at 14:00 UTC, when the rain rate was low (Fig. 14a, b). The temporal variation of the rainwater mixing ratio is similar to the rain rate. The highest peak of rainwater content is seen during 08:00–10:00 UTC, decreasing afterward (Fig. 14c). Overall, the variability of the hydrometeors considered here shows large differences in mixing ratios with different microphysics except for WSM6 and Thompson schemes.

Microphysics significantly influence the rainfall simulation due to variation in mixing ratios of different hydrometeors and the associated dynamic

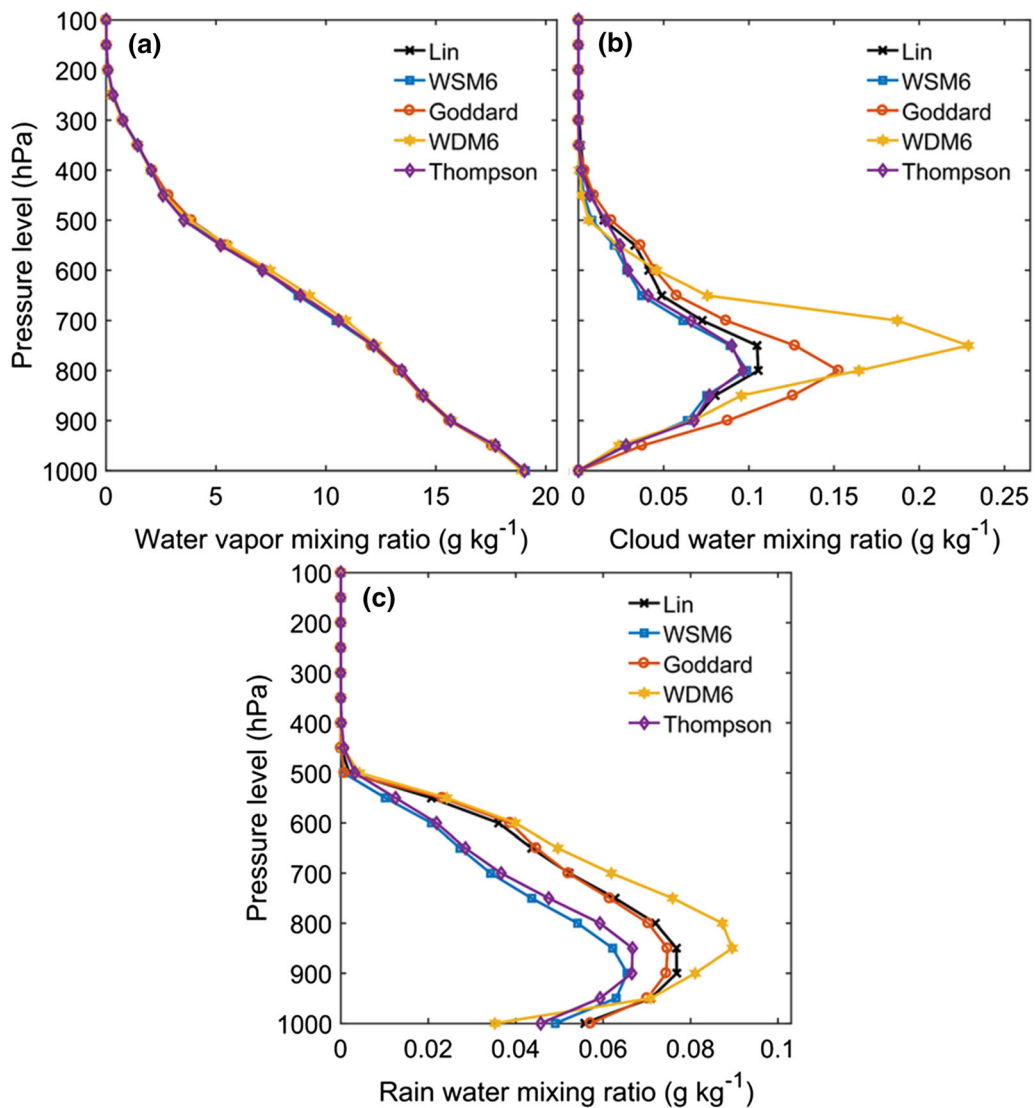


Figure 13

Vertical variation of **a** water mixing ratio, **b** cloud water mixing ratio, and **c** rain water mixing ratio during the 26 August 2016 case

and thermodynamic parameters. Out of five microphysics parameterizations evaluated in this study, the schemes, viz. WSM6, Lin et al., Goddard, and Thompson, captured the initiation time of rainfall occurrence well, while WDM6 showed the rainfall with a lag time of  $> 6$  h (Fig. 11b). The temporal and spatial distribution shows that Lin et al. performed better with relatively smaller statistical errors when ensemble averaging is considered (Table 6). A similar result is found in the case of the single event

of 26 August 2016 with relatively higher IOA for Lin et al. microphysics (Table S1).

With analogous microphysical considerations, except for the cloud ice prognostic variable (Sect. 2.2.2), WSM6 and Thompson behave almost similarly for predicting the rain rate and vertical moisture transport (Fig. 12) and mixing ratios (Figs. 13, 14). However, WDM6 behaved abruptly for predicting these parameters. And Goddard and WDM6 simulated a poor rainfall distribution despite a higher cloud and rainwater mixing ratio (Fig. 13).

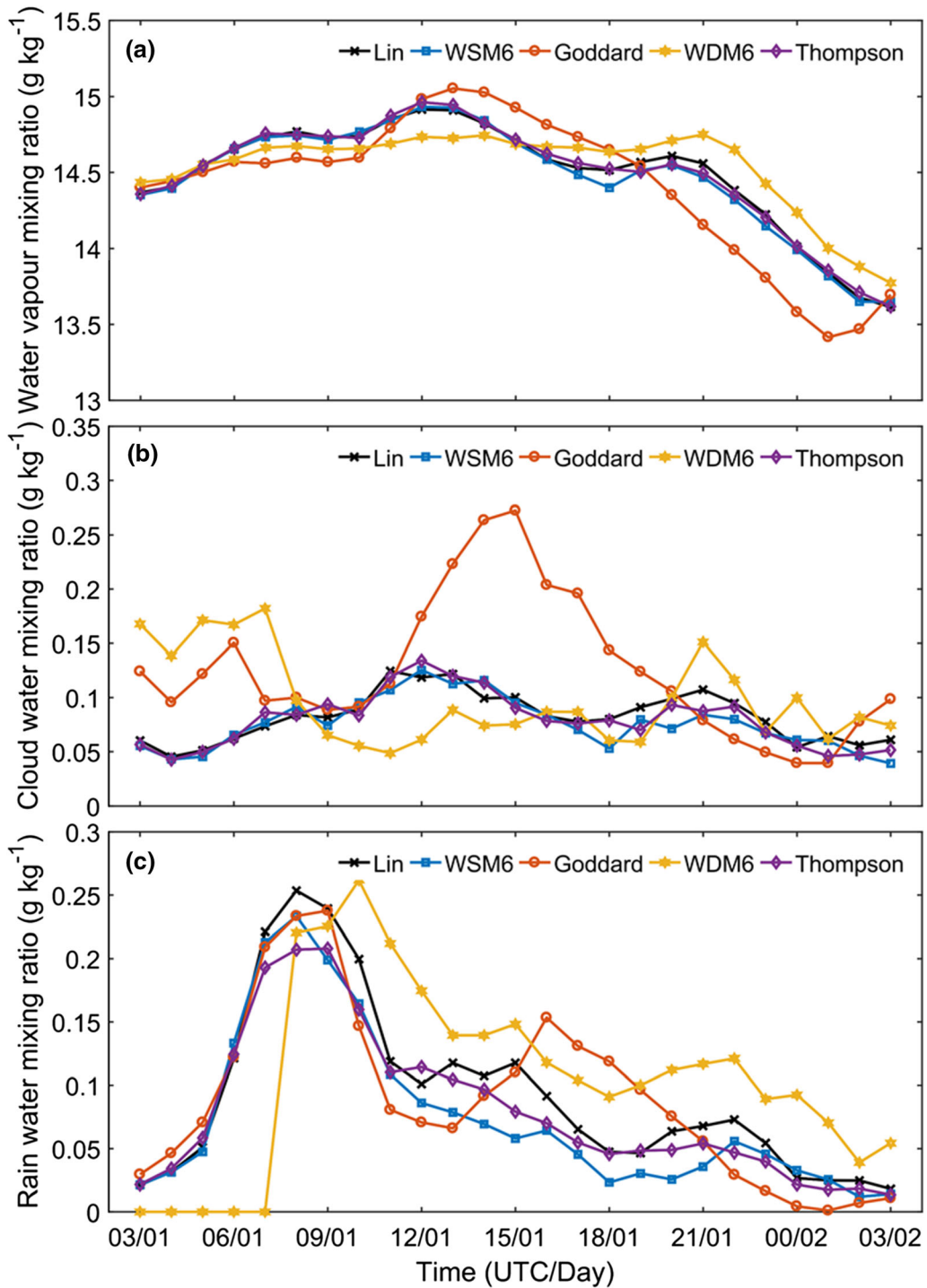


Figure 14

Time series of **a** water vapor mixing ratio, **b** cloud water mixing ratio, and **c** rain water mixing ratio at 850 hPa for different microphysics during the 26 August 2016 case



However, Lin et al. could capture the peak rainfall at 08:00 UTC comparatively well, and relatively higher accumulated rainfall is simulated by it (Figure S7). Irrespective of whether a single case or ensemble-averaged values, Lin et al. microphysics performs relatively better in simulating the rainfall (Figs. 11 and S7; Tables 6 and S1). The variations in hydrometeorological parameters in the case of 26 August 2016 (Figs. 13, 14), and the rain rate and moisture transport variability (Fig. 12) also signify the same. The overall analysis suggested that the Lin et al. scheme is more effective for simulating heavy precipitation events over Mumbai during monsoon. In other parts of the country, either WSM6 (Tiwari et al., 2018), Thompson (Mohan et al., 2018; Rajeevan et al., 2010), or Lin et al. (Rath & Panda, 2020) were found to be working effectively in heavy rainfall scenarios. However, the effectiveness depends on the geographical location, prevailing meteorological conditions, and season of the year. For instance, Mohan et al. (2018) found that the Thompson scheme can produce high vertical motions associated with high instability, considerable mid-level convergence, and high-level divergence during an intense monsoonal precipitation event. Based on the physical considerations, current analysis, and available literature, it may be inferred that Lin et al. microphysics performs better in simulating the intense monsoonal rainfall episodes over coastal cities of India.

#### 4. Conclusions

PBL plays an important role in transforming energy (including momentum, heat, and moisture) into the upper layer of the atmosphere by evaporation and transpiration. However, high vertical mixing transports more moisture from the surface to the free atmosphere and favors the precipitation associated with heavy rainfall events. In contrast, weak vertical mixing confines the moisture to lower levels, which decreases the condensates and corresponding latent heating and reduces the surface precipitation. Therefore, the present study mainly focused on the sensitivity of seven PBL and five microphysics parameterizations in the WRF model, where three

PBL schemes are non-TKE- (YSU, ACM2, and Shin-Hong), and four are TKE- (MYJ, QNSE, BouLac, and GBM) based. And the microphysics schemes considered for sensitivity are primarily based on their types, available literature, and previous experience. For this purpose, 16 intense rainfall scenarios over Mumbai are considered. In total, 176 simulations were carried out to examine the performance of the said PBL and microphysical parameterizations. An ensemble averaging approach was adopted for this purpose.

Comparison of model simulations with ERA5 data for the thermodynamic surface variables (2-m temperature, 10-m wind speed, and sensible and latent heat fluxes) revealed the discrepancies between seven PBL schemes. All the schemes predicted a higher peak during daytime, and the average values in the seven experiments are closer to peak measurements than at nighttime. The results of 2-m temperature and sensible and latent heat fluxes show that the variables diverge (for 2-m temperature) and converge at nighttime, and their values are lower than those observed or those from ERA5. From these results, it was concluded that the representation of surface variables is still uncertain even with the state-of-art PBL schemes. For rainfall, model simulations are compared with the GPM data. The comparison among all the experiments underestimated the rainfall. The highest and lowest rainfall is estimated by QNSE and MYJ, respectively. Statistical analysis of the simulated rainfall with GPM suggests that QNSE (which is TKE-based) has better skills than the rest. The vertical distribution of wind speed shows that wind shear is relatively lower for all the schemes except QNSE. Lower wind shear reduces and higher wind enhances the mixing; therefore, results show a decrease and increase in PBLH for GBM and QNSE, respectively. For all these experiments, the decrease (increase) in the temperature in the mid-troposphere is associated with cooling (heating) due to an increase (decrease) of moisture caused by phase change, except for BouLac. Results for the rainfall,  $T_{2m}$ , and  $RH_{2m}$  over the Mumbai region suggest that the QNSE has comparatively better prediction skills.

QNSE PBL is capable of representing convective conditions like the ones considered in this study. It could produce highly unstable conditions due to

higher CAPE (Coniglio et al., 2013; Hariprasad et al., 2014) and allows strong vertical mixing (Coniglio et al., 2013; Tastula et al., 2015), thereby supporting the formation of a deeper convective boundary layer and deep convective clouds. Therefore, it could predict the near-surface variables comparatively better, although it over-predicted PBLH. However, with higher PBLH, it supports the hypothesis of greater moist instability that is consistent with the prevailing convective condition during the considered rain events. Hence, it helped in producing higher-intensity rainfall compared to other PBL schemes.

The Goddard and WDM6 schemes simulated a poor rainfall distribution despite showing a higher cloud and rainwater mixing ratio. The variability of the hydrometeors considered in this study indicates large differences in mixing ratios between different microphysics except for WSM6 and Thompson schemes. WSM6 and Thompson behaved similarly for the prediction of the rain rate and vertical moisture transport, while WDM6 behaved abruptly. However, the overall analysis indicates that the Lin et al. scheme is effective in accommodating significant vertical motions associated with higher instability in the WRF modeling framework, which is consistent with the capability of QNSE PBL. Therefore, it is concluded that Lin et al. microphysics in combination with QNSE PBL performs relatively better in simulating the intense monsoonal rainfall episodes over coastal regions of India through the advanced research WRF model.

The statistical evaluations in this study suggest a much better WRF model performance for RH compared to temperature and wind speed. However, the WRF model mostly predicts temperature and wind speed much better than the RH over various regions across India (Jain et al., 2021; Panda & Giri, 2012; Panda & Sharan, 2012; Panda et al., 2009; Rath & Panda, 2019, 2020). In the current study, due to far better predictions of RH (in comparison to temperature and wind speed), rainfall predictions are also quite superior in terms of statistical indices such as IOA and others (FB, RMSE, etc.). Some earlier studies highlighted the underestimation or overestimation of near-surface temperature and RH by WRF simulations. For instance, Rao and Rakesh (2019) showed that the WRF model overestimated the near-

surface temperature but underestimated the near-surface RH over Delhi and Hyderabad. Similarly, the studies of Mohan and Bhati (2011), Sati and Mohan (2018), and Mohan and Gupta (2018) reported that the WRF model exhibits a warm bias for near-surface temperature and dry bias for the near-surface RH. Chang et al. (2009) also showed that the simulations considering WRF coupled with the slab and Noah or Noah-based land-surface models tend to over-predict the afternoon temperatures over India. Notably, RH is directly and highly dependent on temperature. Relatively poorer prediction of temperature than RH in the current study may not seem physically consistent. This inconsistency may be attributed to four aspects, which could not be appropriately accounted for in the current simulations, i.e., (a) the altering of LULC distribution pattern due to urbanization (Li et al., 2013, 2016; Ribeiro et al., 2021), (b) unreasonable performance of specific parameterization schemes (Hariprasad et al., 2014), which could not generate the appropriate atmospheric dynamics to represent the actual state of the atmosphere (Banks et al., 2016), (c) wetness of the soil, and (d) seasonality that determines the receipt of rainfall by a particular region to help increase the moisture availability in the soil and atmosphere. Notably, the incorporation of high-resolution LULC data with different urban classes (Li et al., 2013, 2016) in the WRF urban canopy model and the accurate estimation of surface heat and moisture fluxes (Srivastava & Sharan, 2017) may alter the model bias over highly urbanized pockets (Bhimala et al., 2021). Although the present study showed a better rainfall prediction by WRF simulations during monsoonal intense rainfall events, the predictability may be improved further with higher-resolution ( $\sim 1$  km) configurations by considering better resolved PBL, convection, and topographic features. Data assimilation techniques may be adopted to assimilate land surface and atmospheric parameters to help improve the model predictability.

#### *Acknowledgements*

The authors want to express their gratitude to the National Aeronautics and Space Administration

(NASA) Precipitation Measurements Mission (GPM) for providing the half-hourly rainfall data (<https://gpm.nasa.gov/data-access/downloads/gpm>), National Centers for Environmental Prediction (NCEP) for initial and National Center for Atmospheric Research for global FNL data (<https://rda.ucar.edu/datasets/ds083.2/>), European Center for Medium-Range Weather Forecasts (ECMWF) for providing high-resolution ERA5 reanalysis data (<https://www.ecmwf.int/en/forecasts/datasets/reanalysis-datasets/era5>), and weather underground (<https://www.wunderground.com/>) and Wyoming weather web (<http://weather.uwyo.edu/upperair/>) for providing station observations to validate the WRF model simulations.

**Author Contributions** SV wrote the initial draft. The figures were produced by Dr. SSR and SV. The simulations were jointly planned by all authors and carried out by SSR and SV. The primary idea of the work was of Dr. JP, who helped in manuscript writing, editing, and supervising. All the resources for executing the work were arranged by Dr. JP.

### Funding

This work was partly funded through the sponsored project by the Science and Engineering Research Board, Department of Science and Technology, Government of India with file no. EMR/2015/001358.

### Declarations

**Conflict of Interest** There are no scientific or financial conflicts of interest among the contributing authors.

**Publisher's Note** Springer Nature remains neutral with regard to jurisdictional claims in published maps and institutional affiliations.

### REFERENCES

- Alapaty, K., Pleim, J. E., Raman, S., Niyogi, D. S., & Byun, D. W. (1997). Simulation of atmospheric boundary layer processes using local-and nonlocal-closure schemes. *Journal of Applied Meteorology*, 36(3), 214–233.
- Banks, R. F., Tiana-Alsina, J., Baldasano, J. M., Rocadenbosch, F., Papayannis, A., Solomos, S., & Tzani, C. G. (2016). Sensitivity of boundary-layer variables to PBL schemes in the WRF model based on surface meteorological observations, lidar, and radiosondes during the HygrA-CD campaign. *Atmospheric Research*, 176, 185–201.
- Bhimala, K. R., Gouda, K. C., & Himesh, S. (2021). Evaluating the spatial distribution of WRF-simulated rainfall, 2-m air temperature, and 2-m relative humidity over the urban region of Bangalore, India. *Pure and Applied Geophysics*, 178(3), 1105–1120.
- Boadh, R., Satyanarayana, A. N. V., Krishna, T. R., & Madala, S. (2016). Sensitivity of PBL schemes of the WRF-ARW model in simulating the boundary layer flow parameters for their application to air pollution dispersion modeling over a tropical station. *Atmosfera*, 29(1), 61–81.
- Borrego, C., Monteiro, A., Ferreira, J., Miranda, A. I., Costa, A. M., Carvalho, A. C., & Lopes, M. (2008). Procedures for estimation of modelling uncertainty in air quality assessment. *Environment International*, 34(5), 613–620.
- Bougeault, P., & Lacarrere, P. (1989). Parameterization of orography-induced turbulence in a mesobeta-scale model. *Monthly Weather Review*, 117(8), 1872–1890.
- Braun, S. A., & Tao, W. K. (2000). Sensitivity of high-resolution simulations of Hurricane Bob (1991) to planetary boundary layer parameterizations. *Monthly Weather Review*, 128(12), 3941–3961.
- Bright, D. R., & Mullen, S. L. (2002). The sensitivity of the numerical simulation of the southwest monsoon boundary layer to the choice of PBL turbulence parameterization in MM5. *Weather and Forecasting*, 17(1), 99–114.
- Chang, H. I., Kumar, A., Niyogi, D., Mohanty, U. C., Chen, F., & Dudhia, J. (2009). The role of land surface processes on the mesoscale simulation of the July 26, 2005 heavy rain event over Mumbai, India. *Global and Planetary Change*, 67(1–2), 87–103.
- Coniglio, M. C., Correia, J., Jr., Marsh, P. T., & Kong, F. (2013). Verification of convection-allowing WRF model forecasts of the planetary boundary layer using sounding observations. *Weather and Forecasting*, 28(3), 842–862.
- Cooper, W. A. (1986). *Ice initiation in natural clouds. In Precipitation enhancement—a scientific challenge* (pp. 29–32). American Meteorological Society.
- Deng, A., & Stauffer, D. R. (2006). On improving 4-km mesoscale model simulations. *Journal of Applied Meteorology and Climatology*, 45(3), 361–381.
- Dawn, S., & Satyanarayana, A. N. V. (2020). Sensitivity studies of cloud microphysical schemes of WRF-ARW model in the simulation of trailing stratiform squall lines over the Gangetic West Bengal region. *Journal of Atmospheric and Solar-Terrestrial Physics*, 209, 105396.
- Efstathiou, G. A., Zoumakis, N. M., Melas, D., Lolis, C. J., & Kassomenos, P. (2013). Sensitivity of WRF to boundary layer parameterizations in simulating a heavy rainfall event using different microphysical schemes. *Effect on Large-Scale Processes. Atmospheric Research*, 132, 125–143.
- Emery, C.A. (2001). Enhanced meteorological modeling and performance evaluation for two Texas ozone episodes. Texas Natural Resource Conservation Commission, ENVIRON International Corporation, pp. 1–235. <http://www.tceq.state.tx.us/assets/public/implementation/air/am/contracts/reports/mm/EnhancedMetModelingAndPerformanceEvaluation.pdf>.
- Galperin, B., & Sukoriansky, S. (2010). Progress in turbulence parameterization for geophysical flows. In *The 3rd international workshop on Next-generation NWP models: bridging*

- parameterization, explicit clouds, and large eddies. Seoul, Korea (Vol. 5).
- Garratt, J. R. (1994). The atmospheric boundary layer. *Earth-Science Reviews*, 37(1–2), 89–134.
- Gilliam, R. C., Hogrefe, C., & Rao, S. T. (2006). New methods for evaluating meteorological models used in air quality applications. *Atmospheric Environment*, 40(26), 5073–5086.
- Gordon, N. D., & Shaykewich, J. (2000). *Guidelines on performance assessment of public weather services*. World Meteorological Organization, WMO/TD No. 1023, pp. 1–67. [https://www.wmo.int/pages/prog/hwrf/documents/FFI/expert/Guidelines\\_on\\_Performance\\_Assessment\\_of\\_Public\\_Weather\\_Services.pdf](https://www.wmo.int/pages/prog/hwrf/documents/FFI/expert/Guidelines_on_Performance_Assessment_of_Public_Weather_Services.pdf)
- Grenier, H., & Bretherton, C. S. (2001). A moist PBL parameterization for large-scale models and its application to subtropical cloud-topped marine boundary layers. *Monthly Weather Review*, 129(3), 357–377.
- Gunwani, P., & Mohan, M. (2017). Sensitivity of WRF model estimates to various PBL parameterizations in different climatic zones over India. *Atmospheric Research*, 194, 43–65.
- Hariprasad, K. B. R. R., Srinivas, C. V., Singh, A. B., Rao, S. V. B., Baskaran, R., & Venkatraman, B. (2014). Numerical simulation and intercomparison of boundary layer structure with different PBL schemes in WRF using experimental observations at a tropical site. *Atmospheric Research*, 145, 27–44.
- Hong, S. Y., & Lim, J. O. J. (2006). The WRF single-moment 6-class microphysics scheme (WSM6). *Asia-Pacific Journal of Atmospheric Sciences*, 42(2), 129–151.
- Hong, S. Y., Lim, K. S. S., Lee, Y. H., Ha, J. C., Kim, H. W., Ham, S. J., & Dudhia, J. (2010). Evaluation of the WRF double-moment 6-class microphysics scheme for precipitating convection. *Advances in Meteorology*. <https://doi.org/10.1155/2010/707253>
- Hong, S. Y., & Pan, H. L. (1996). Non-local boundary layer vertical diffusion in a medium-range forecast model. *Monthly Weather Review*, 124(10), 2322–2339.
- Igri, P. M., Tanessong, R. S., Vondou, D. A., Panda, J., Garba, A., Mkankam, F. K., & Kamga, A. (2018). Assessing the performance of WRF model in predicting high-impact weather conditions over Central and Western Africa: An ensemble-based approach. *Natural Hazards*, 93(3), 1565–1587.
- Jain, S., Roy, S. B., Panda, J., & Rath, S. S. (2021). Modeling of land-use and land-cover change impact on summertime near-surface temperature variability over the Delhi-Mumbai Industrial Corridor. *Modeling Earth Systems and Environment*, 7(2), 1309–1319.
- Janjić, Z. I. (1990). The step-mountain coordinate: Physical package. *Monthly Weather Review*, 118(7), 1429–1443.
- Janjić, Z. I. (1994). The step-mountain eta coordinate model: Further developments of the convection, viscous sublayer, and turbulence closure schemes. *Monthly Weather Review*, 122(5), 927–945.
- Janjić, Z. I. (2000). Comments on “Development and evaluation of a convection scheme for use in climate models.” *Journal of the Atmospheric Sciences*, 57(21), 3686–3686.
- Kumar, A., Dudhia, J., Rotunno, R., Niyogi, D., & Mohanty, U. C. (2008). Analysis of the 26 July 2005 heavy rain event over Mumbai, India using the Weather Research and Forecasting (WRF) model. *Quarterly Journal of the Royal Meteorological Society*, 134(636), 1897–1910.
- Lang, S., Tao, W. K., Simpson, J., Cifelli, R., Rutledge, S., Olson, W., et al. (2007). Improving simulations of convective systems from TRMM LBA: Easterly and westerly regimes. *Journal of the atmospheric sciences*, 64(4), 1141–1164.
- Li, X. X., Koh, T. Y., Entekhabi, D., Roth, M., Panda, J., & Norford, L. K. (2013). A multi-resolution ensemble study of a tropical urban environment and its interactions with the background regional atmosphere. *Journal of Geophysical Research: Atmospheres*, 118(17), 9804–9818.
- Li, X. X., Koh, T. Y., Panda, J., & Norford, L. K. (2016). Impact of urbanization patterns on the local climate of a tropical city, Singapore: An ensemble study. *Journal of Geophysical Research: Atmospheres*, 121(9), 4386–4403.
- Lim, K. S. S., & Hong, S. Y. (2010). Development of an effective double-moment cloud microphysics scheme with prognostic cloud condensation nuclei (CCN) for weather and climate models. *Monthly Weather Review*, 138(5), 1587–1612.
- Lin, Y. L., Farley, R. D., & Orville, H. D. (1983). Bulk parameterization of the snow field in a cloud model. *Journal of Climate and Applied Meteorology*, 22(6), 1065–1092.
- Liu, Y., & Avissar, R. (1996). Sensitivity of shallow convective precipitation induced by land surface heterogeneities to dynamical and cloud microphysical parameters. *Journal of Geophysical Research: Atmospheres*, 101(D3), 7477–7497.
- Mitchell, D. L., Rasch, P., Ivanova, D., McFarquhar, G., & Nousiainen, T. (2008). Impact of small ice crystal assumptions on ice sedimentation rates in cirrus clouds and GCM simulations. *Geophysical Research Letters*, 35(9).
- Moeng, C. H. (1984). A large-eddy-simulation model for the study of planetary boundary-layer turbulence. *Journal of the Atmospheric Sciences*, 41(13), 2052–2062.
- Mohan, M., & Bhati, S. (2011). Analysis of WRF model performance over subtropical region of Delhi, India. *Advances in Meteorology*. <https://doi.org/10.1155/2011/621235>
- Mohan, M., & Gupta, M. (2018). Sensitivity of PBL parameterizations on PM10 and ozone simulation using chemical transport model WRF-Chem over a sub-tropical urban airshed in India. *Atmospheric Environment*, 185, 53–63.
- Mohan, P. R., Srinivas, C. V., Yesubabu, V., Baskaran, R., & Venkatraman, B. (2018). Simulation of a heavy rainfall event over Chennai in Southeast India using WRF: Sensitivity to microphysics parameterization. *Atmospheric Research*, 210, 83–99.
- Orr, A., Listowski, C., Coustet, M., Collier, E., Immerzeel, W., Deb, P., & Bannister, D. (2017). Sensitivity of simulated summer monsoonal precipitation in Langtang Valley, Himalaya, to cloud microphysics schemes in WRF. *Journal of Geophysical Research: Atmospheres*, 122(12), 6298–6318.
- Panda, J., & Giri, R. K. (2012). A comprehensive study of surface and upper-air characteristics over two stations on the west coast of India during the occurrence of a cyclonic storm. *Natural Hazards*, 64(2), 1055–1078.
- Panda, J., & Sharan, M. (2012). Influence of land-surface and turbulent parameterization schemes on regional-scale boundary layer characteristics over northern India. *Atmospheric Research*, 112, 89–111.
- Panda, J., Sharan, M., & Gopalakrishnan, S. G. (2009). Study of regional-scale boundary layer characteristics over Northern India with a special reference to the role of the Thar Desert in regional-scale transport. *Journal of Applied Meteorology and Climatology*, 48(11), 2377–2402.
- Persson, P., Walter, B., Bao, J. W., & Michelson, S. (2001). Validation of boundary-layer parameterizations in maritime storm

- using aircraft data. Preprints. In Ninth Conf. on Mesoscale Processes (pp. 117–121).
- Pieri, A. B., von Hardenberg, J., Parodi, A., & Provenzale, A. (2015). Sensitivity of precipitation statistics to resolution, microphysics, and convective parameterization: A case study with the high-resolution WRF climate model over Europe. *Journal of Hydrometeorology*, 16(4), 1857–1872.
- Pleim, J. E. (2007). A combined local and non-local closure model for the atmospheric boundary layer. Part II: Application and evaluation in a mesoscale meteorological model. *Journal of Applied Meteorology and Climatology*, 46(9), 1396–1409.
- Rai, D., & Pattnaik, S. (2019). Evaluation of WRF planetary boundary layer parameterization schemes for simulation of monsoon depressions over India. *Meteorology and Atmospheric Physics*. <https://doi.org/10.1007/s00703-019-0656-3>
- Rajeevan, M., Kesarkar, A., Thampi, S. B., Rao, T. N., Radhakrishna, B., & Rajasekhar, M. (2010). Sensitivity of WRF cloud microphysics to simulations of a severe thunderstorm event over Southeast India. *Annales Geophysicae*, 28(2), 603–619.
- Rao, B. K., & Rakesh, V. (2019). Evaluation of WRF-simulated multilevel soil moisture, 2-m air temperature, and 2-m relative humidity against in situ observations in India. *Pure and Applied Geophysics*, 176(4), 1807–1826.
- Rath, S. S., & Panda, J. (2019). A study of near-surface boundary layer characteristics during the 2015 Chennai flood in the context of urban-induced land use changes. *Pure and Applied Geophysics*, 176(6), 2607–2629.
- Rath, S. S., & Panda, J. (2020). Urban induced land-use change impact during pre-monsoon thunderstorms over Bhubaneswar-Cuttack urban complex. *Urban Climate*, 32, 100628.
- Ribeiro, I., Martilli, A., Falls, M., Zonato, A., & Villalba, G. (2021). Highly resolved WRF-BEP/BEM simulations over Barcelona urban area with LCZ. *Atmospheric Research*, 248, 105220.
- Rutledge, S. A., & Hobbs, P. V. (1984). The mesoscale and microscale structure and organization of clouds and precipitation in midlatitude cyclones. XII: A diagnostic modeling study of precipitation development in narrow cold-frontal rainbands. *Journal of the Atmospheric Sciences*, 41(20), 2949–2972.
- Sathyanadh, A., Prabha, T. V., Balaji, B., Resmi, E. A., & Karipot, A. (2017). Evaluation of WRF PBL parameterization schemes against direct observations during a dry event over the Ganges valley. *Atmospheric Research*, 193, 125–141.
- Sati, A. P., & Mohan, M. (2018). The impact of urbanization during half a century on surface meteorology based on WRF model simulations over National Capital Region, India. *Theoretical and Applied Climatology*, 134(1), 309–323.
- Schlünzen, K. H., & Sokhi, R. S. (2008). Overview of tools and methods for meteorological and air pollution mesoscale model evaluation and user training. *Joint Report by WMO and COST*, 728, 116.
- Shin, H. H., & Hong, S. Y. (2011). Intercomparison of planetary boundary-layer parametrizations in the WRF model for a single day from CASES-99. *Boundary-Layer Meteorology*, 139(2), 261–281.
- Shin, H. H., & Hong, S. Y. (2015). Representation of the subgrid-scale turbulent transport in convective boundary layers at gray-zone resolutions. *Monthly Weather Review*, 143(1), 250–271.
- Singh, K. S., Bonthu, S., Purvaja, R., Robin, R. S., Kannan, B. A. M., & Ramesh, R. (2018). Prediction of heavy rainfall over Chennai Metropolitan City, Tamil Nadu, India: Impact of microphysical parameterization schemes. *Atmospheric Research*, 202, 219–234.
- Skamarock, W. C., & Klemp, J. B. (1992). The stability of time-split numerical methods for the hydrostatic and the nonhydrostatic elastic equations. *Monthly Weather Review*, 120(9), 2109–2127.
- Skamarock, W. C., Klemp, J. B., Dudhia, J., Gill, D. O., Barker, D. M., Duda, M. G., et al. (2008). A description of the advanced research WRF, Version 3, Technical report, NCAR/TN-475+STR.
- Skamarock, W. C., Klemp, J. B., Dudhia, J., Gill, D. O., Barker, D. M., Wang, W., & Powers, J. G. (2005). A description of the advanced research WRF version 2 (No. NCAR/TN-468+STR). National Center for Atmospheric Research Boulder Co Mesoscale and Microscale Meteorology Div.
- Srinivas, C. V., Yesubabu, V., Prasad, D. H., Prasad, K. H., Greeshma, M. M., Baskaran, R., & Venkatraman, B. (2018). Simulation of an extreme heavy rainfall event over Chennai, India using WRF: Sensitivity to grid resolution and boundary layer physics. *Atmospheric Research*, 210, 66–82.
- Srinivas, G., Remya, P. G., Kumar, B. P., Modi, A., & Nair, T. B. (2020). The impact of Indian Ocean Dipole on tropical Indian Ocean surface wave heights in ERA5 and CMIP5 models. *International Journal of Climatology*. <https://doi.org/10.1002/joc.6900>
- Srivastava, P., & Sharan, M. (2017). An analytical formulation of the Monin-Obukhov stability parameter in the atmospheric surface layer under unstable conditions. *Boundary-Layer Meteorology*, 165(2), 371–384.
- Stensrud, D. J. (2009). *Parameterization schemes: Keys to understanding numerical weather prediction models*. Cambridge University Press.
- Stensrud, D. J., & Weiss, S. J. (2002). Mesoscale model ensemble forecasts of the 3 May 1999 tornado outbreak. *Weather and Forecasting*, 17(3), 526–543.
- Stull, R. B. (1988). *Mean boundary layer characteristics*. In *An introduction to boundary layer meteorology* (pp. 1–27). Springer.
- Stull, R. B. (1991). Static stability—an update. *Bulletin of the American Meteorological Society*, 72(10), 1521–1530.
- Stull, R. B. (2012). *An introduction to boundary layer meteorology* (Vol. 13). Springer Science & Business Media.
- Sukoriansky, S., Galperin, B., & Staroselsky, I. (2005). A quasi-normal scale elimination model of turbulent flows with stable stratification. *Physics of Fluids*, 17(8), 085107.
- Tao, W. K., & Simpson, J. (1993). The Goddard cumulus ensemble model. Part I: Model description. *Terrestrial, Atmospheric and Oceanic Sciences*, 4(1), 35–72.
- Tao, W. K., Simpson, J., Baker, D., Braun, S., Chou, M. D., Ferrier, B., et al. (2003). Microphysics, radiation and surface processes in the Goddard Cumulus Ensemble (GCE) model. *Meteorology and Atmospheric Physics*, 82(1), 97–137.
- Tao, W. K., Simpson, J., & McCumber, M. (1989). An ice-water saturation adjustment. *Monthly Weather Review*, 117(1), 231–235.
- Tarek, M., Brissette, F. P., & Arsenault, R. (2020). Evaluation of the ERA5 reanalysis as a potential reference dataset for hydrological modelling over North America. *Hydrology and Earth System Sciences*, 24(5), 2527–2544.
- Tastula, E. M., Galperin, B., Dudhia, J., LeMone, M. A., Sukoriansky, S., & Vihma, T. (2015). Methodical assessment of the differences between the QNSE and MYJ PBL schemes for

- stable conditions. *Quarterly Journal of the Royal Meteorological Society*, 141(691), 2077–2089.
- Thompson, G., Rasmussen, R. M., & Manning, K. (2004). Explicit forecasts of winter precipitation using an improved bulk microphysics scheme. Part I: Description and sensitivity analysis. *Monthly Weather Review*, 132(2), 519–542.
- Tiwari, S., Kar, S. C., & Bhatla, R. (2018). Dynamic downscaling over western Himalayas: Impact of cloud microphysics schemes. *Atmospheric Research*, 201, 1–16.
- Walko, R. L., Cotton, W. R., Meyers, M. P., & Harrington, J. Y. (1995). New RAMS cloud microphysics parameterization part I: The single-moment scheme. *Atmospheric Research*, 38(1–4), 29–62.
- Wang, W., Barker, D., Bruyere, C., Dudhia, J., Gill, D., and Michalakes, J. (2004). WRF Version 2 modeling system user's guide, <http://www.mmm.ucar.edu/wrf/users/docs/userguide/>.
- Wang, W., Beezley, C., & Duda, M. (2012). WRF ARW V3: user's guide. Wang, C. Beezley, M. Duda, et al. <http://www.mmm.ucar.edu/wrf/users> (accessed: 11.01. 2013).
- Wang, W., Bruyere, C., Duda, M., Dudhia, J., Gill, D., Kavulich, M., Rizvi, S., & et al. (2017). User's Guides for the Advanced Research WRF (ARW) Modeling System. Version 3. [https://www2.mmm.ucar.edu/wrf/users/docs/user\\_guide\\_V3/user\\_guide\\_V3.8/ARWUsersGuideV3.8.pdf](https://www2.mmm.ucar.edu/wrf/users/docs/user_guide_V3/user_guide_V3.8/ARWUsersGuideV3.8.pdf).
- Wang, Y., Feng, J., Luo, M., Wang, J., & Qiu, Y. (2020). Uncertainties in simulating central Asia: Sensitivity to physical parameterizations using Weather Research and Forecasting model. *International Journal of Climatology*, 40(14), 5813–5828.
- Weisman, M. L., Davis, C., Wang, W., Manning, K. W., & Klemp, J. B. (2008). Experiences with 0–36-h explicit convective forecasts with the WRF-ARW model. *Weather and Forecasting*, 23(3), 407–437.
- Willmott, C. J. (1981). On the validation of models. *Physical Geography*, 2, 184–194.
- Wisse, J. S. P., & de Arellano, J. V. G. (2004). Analysis of the role of the planetary boundary layer schemes during a severe convective storm. *Annales Geophysicae*, 22(6), 1861–1874.
- Zeng, X., Tao, W. K., Lang, S., Hou, A. Y., Zhang, M., & Simpson, J. (2008). On the sensitivity of atmospheric ensembles to cloud microphysics in long-term cloud-resolving model simulations. *Journal of the Meteorological Society of Japan Series II*, 86, 45–65.
- Zeng, X., Tao, W. K., Zhang, M., Hou, A. Y., Xie, S., Lang, S., et al. (2009). An indirect effect of ice nuclei on atmospheric radiation. *Journal of the Atmospheric Sciences*, 66(1), 41–61.
- Zhang, D. L., & Zheng, W. Z. (2004). Diurnal cycles of surface winds and temperatures as simulated by five boundary layer parameterizations. *Journal of Applied Meteorology*, 43(1), 157–169.

(Received September 1, 2020, revised June 27, 2021, accepted June 29, 2021, Published online July 12, 2021)